A Biologically Inspired Controllable Stiffness Multimodal Whisker Follicle

R N Brahmana Panditha Mudiyanse Ralahami, Hasitha

Awarding institution:
King's College London

SCHOOL OF NATURAL AND
MATHEMATICAL SCIENCES

DEPARTMENT OF INFORMATICS

THESIS

A Biologically Inspired Controllable Stiffness Multimodal Whisker Follicle

Author:
Hasitha Bandara Wegiriya.

Research Advisor:
Prof. Thrishantha Nanayakkara

April 2021

Abstract

This thesis takes a soft robotics approach to understand the computational role of a soft whisker follicle with mechanisms to control the stiffness of the whisker. In particular, the thesis explores the role of the controllable stiffness whisker follicle to selectively favour low frequency geometric features of an object or the high frequency texture features of the object.

Tactile sensing is one of the most essential and complex sensory systems for most living beings. To acquire tactile information and explore the environment, animals use various biological mechanisms and transducing techniques. Whiskers, or vibrissae are a form of mammalian hair, found on almost all mammals other than homo sapiens. For many mammals, and especially rodents, these whiskers are essential as a means of tactile sensing.

The mammalian whisker follicle contains multiple sensory receptors strategically organised to capture tactile sensory stimuli of different frequencies via the vibrissal system. Nocturnal mammals such as rats heavily depend on whisker based tactile perception to find their way through burrows and identify objects. There is diversity in the whiskers in terms of the physical structure and nervous innervation. The robotics community has developed many different whisker sensors inspired by this biological basis. They take diverse mechanical, electronic, and computational approaches to use whiskers to identify the geometry, mechanical properties, and objects' texture. Some work addresses specific object identification features and others address multiple features such as texture and shape etc. Therefore, it is vital to have a comprehensive discussion of the literature and to understand the merits of bio-inspired and pure-engineered approaches to whisker-based tactile perception.

The most important contribution is the design and use of a novel soft whisker follicle comprising two different frequency-dependent data capturing modules to derive more profound insights into the biological basis of tactile perception in the mammalian whisker follicle. The new insights into the biological basis of tactile perception using whiskers provide new design guidelines to develop efficient robotic whiskers.

Dedication

To my loving parents and my loving wife.

Acknowledgements

Firstly, I would like to express my gratitude to my research supervisor Professor Thrishantha Nanayakkara for all his support, dedication, advice, and opportunities, which has empowered me to grow into an independent researcher. It is my great honour to perform research and work with him.

I would also like to thank my King's College London supervisor Dr Hongbin Liu and Professor Elizabeth Sklar for their support during my study.

I want to give special thanks to Morph Lab and Imperial College London for their support, I received during my research.

I would also like to thank Prof Kaspar Althoefer for his support during my first year at King's College London.

I sincerely appreciate my mother Chithrani Abayrathene Bandara, and my father Abayrathene Bandara for their love and support throughout my study and research.

I want to give special gratitude to my loving wife Niluka Wegiriya for giving me constant support and motivation.

I want to thank my colleagues and friends Dr Nicolas Herzig, Dr Sara Abad Guaman, Dr S.M.Hadi Sadati, Dr Liang He, Dr Saina Akhond, Dr Nantachai Sornkarn, Dr Thilina Dulantha Lalitharatne, Dr Anuradha Ranasinghe, Dr Ali Shiva, Dr Visakha Nanayakkara, Dr Elham Hamid, Harry Bedford, Zhenhua Yu and all the other members of the Dyson School of Design Engineering and King's College London for their support and all the valuable discussions during all these years. It has been a great pleasure to work with everyone.

I also want to thank all my friends and family for being there for me during my studies in the UK.

Declaration

I hereby declare that this thesis and the work reported herein was composed by and originated entirely by me. Information derived from the published and unpublished work of others has been acknowledged in the text, and references have been given in the list of sources.

Hasitha Bandara Wegiriya R N B P Mudiyanse Ralahamilage

April 2021

Contents

Abstract **i**

Acknowledgements **v**

1 Introduction **1**

1.1 Literature Review 2

1.1.1 Biological Description of the Whisker Follicle 3

1.1.2 Biological Inspiration for Artificial Whisker Sensors 5

1.1.3 Objects Shape Detection and Recognition 7

1.1.4 Texture Recognition and Classification of Objects 8

1.1.5 Obstacles Detection, and Location for navigation 9

1.2 Research questions 10

1.3 Research Contributions 11

1.4 Publications 11

1.4.1 Conference Papers 11

1.4.2 Journal Papers 12

2 Multimodal Whisker Follicle **13**

2.1 Sensor Design 14

2.1.1 Characterisation of the Sensor 15

2.1.2 Experimental Setup 16

2.1.3 Experiment Process 16

2.2 Results 17

3 Stiffness Controllable Multimodal Whisker Follicle **23**

3.1 Introduction of the Stiffness Controllable Whisker Follicle 24

3.2 Experimental Methodology 25

3.2.1 Characterisation of the Sensor 26

3.2.2 Experiment Setup 26

3.2.3 Experiment Process 28

3.3 Results 30

4 Extended study of Stiffness Controllable Multimodal Whisker Follicle **38**

4.0.1 Stiffness Controllable Multimodal Whisker Sensor Characterization . . . 39

4.0.2 Whisker Modal Analysis 40

4.0.3 Experiment Setup 42

4.0.4 Calculation of distance between distribution of textures 45

4.1 RESULTS 46

4.1.1 Numerical simulation results 46

4.1.2 Signal amplitude variation with follicle stiffness and free oscillation frequency 46

4.1.3 Maximizing a difference metric for texture classification 48

4.1.4 Angle Dependent Stiffness in the Whisker Follicle Helps to Arbitrate Multimodal Vibrisal Perception 51

5 Conclusion **54**

5.1 Summary of the Research Achievements 54

Bibliography **58**

List of Tables

1.1 A summary of published whisker tactile sensor 7

List of Figures

1.1 Examples of Whiskered animals: a) The mouse has whisker grid of five rows on each side of the snout, each row containing five to nine whiskers ranging between 15 and 50 mm in length. These whiskers help them for survival such as finding food escaping from predators. b) The cat whisker help them guiding in a limited environment such as moving through small hole and locating their food. 2

1.2 Visual representation showing a timeline of whisker base research evaluation in time 3

1.3 Anatomy of the rat whisker follicle (Diamond and Ehsan 2013). 4

1.4 The layout map summarises the research development of whiskers. 5

2.1 Constructed Whisker Sensor. The hall sensor is mounted inside the cylindrical body. The back end of the carbon fiber shaft is attached to a component connector through the piezoelectric sensor which holds the permanent magnet. The distance between the hall sensor and the permanent magnet was optimized based on the flux induced by the magnet. 14

2.2 Experimental Setup, (i.) Hardware Setup, (ii.) Plastic Pipe, (iii.) Programmed Path - ABCD (Data recording starts when the Whisker shaft moving from A position to B, then data recording stops and sensor goes on the B,C,D route. When the sensor moving from D to A, program select the contact indentation and selected indentation added to D to A distance, then proceed on the square path.) 15

2.3 Hall sensor readings for two speeds and two indentation levels of brushing the whisker against the object in a constant distance shown in figure 2.2. The experiments were conducted for 5 speeds and 6 indentation levels. The plots show data from 20 trials for each speed-indentation combination. The plot C and D samples ten times less due to the speed. 17

2.4 Piezoelectric sensor readings for two speeds and two indentation levels of brushing the whisker against the object in a constant distance shown in figure 2.2. The plots show data from 20 trials for each speed-indentation combination.The plot C and D samples ten times less due to the speed. 18

2.5 The co-variation of hall sensor and piezosensor data across 5 speeds for all 6 indentation levels. 19

2.6 The stranded deviation of piezosensor data across 5 speeds for all 6 indentation levels. 20

2.7 The co-variation of hall sensor and piezosensor data across 6 indentation levels for all 5 speed levels. 21

2.8 Average behavior of maximum eigenvalues of the covariance matrix for hall sensor and piezosensor readings across different indentation levels and speeds of brushing the whisker. 22

2.9 The transfer entropy measured by the information gained during the variation of indentation levels across different whisker's speed levels 22

3.1 Whisker follicle. (A) Schematic illustration of the structure innervation of a rat whisker follicle [1]; V, vibrissal shaft; RS, ring sinus; SVN, superficial vibrissal nerve; DVN, deep vibrissal nerve. (B) Cross section of the variable stiffness multimodal whisker follicle (VS-MWF); CFWS, carbon fibre whisker shaft; PS, piezoelectric sensor; ST, silicone tube; CFR, carbon fibre rod (It has four); SJ, silicon joint; SRM, steering ring mechanism; WSB, whisker shaft base; HS, hall sensor; SL, string link; LA, linear actuator; PM, permanent magnate; CB, 3D printed Cylindrical body. (C) Complete VS-MWF; S, spring. The spring is used to relocate the SRM, when the LA is decreasing the actuated length. (D) Enlarged VS-MWF to demonstrate the stiffness controllable system. 25

3.2 Experimental Setup, (A) Hardware Setup and Programmed Path; Hardware Setup - (a) Power supply (b) Controller of the XY linear stage, (c) Data acquisition (DAQ), (d) XY linear stage (e) Emergency stop switch, (f) VS-MWF (g) Sandpaper holder, Programmed Path is $p1$,$p2$,$p3$ and $p4$ (Data recording starts when the Whisker shaft moving from $p1$ position to $p2$, then data recording stops and sensor goes on the $p2, p3, p4$ route), (B) variable stiffness multimodal whisker follicle (VS-MWF) probing against a sandpaper 27

3.3 Raw data of Hall sensor for different frequencies and stiffness. The red line refers to the first trial, the blue line refers to the second trial. 30

3.4 Raw data of piezo sensor for different frequencies and stiffness. The red line refers to the first trial, the blue line refers to the second trial. 31

3.5 The colorbar represents the root mean square (RMS) of Hall sensor with stiffness level and frequency [Hz]. Stiffness levels are relative to the linear actuator displacement from 0 mm (stiffness level 1) to 16 mm (stiffness level 9) by 2 mm rises. 32

3.6 The colorbar represents the root mean square (RMS) of Piezo sensor with stiffness level and frequency [Hz]. Stiffness levels are relative to the linear actuator displacement from 0 mm (stiffness level 1) to 16 mm (stiffness level 9) by 2 mm rises. 33

3.7 Covariance of Piezoelectric and Hall sensor with stiffness and frequency. Red and blue ellipses refer to trials 1 and 2 respectively. Axis ranges are not shown for clarity. Both x and y axises range from -0.02 to 0.02 34

3.8 Covariance of Piezo and Hall sensor with stiffness and Speed for two materials. The red curves refer to the bins of the 3000 grit sandpaper, the blue curves refer to 5000 grit sandpaper. 35

3.9 The probability distributions of Frobenius distance at a stiffness level and whisking speed. whisking speeds are 10mm/s for speed 1, 14mm/s speed 2 and 18mm/s speed 3. Stiffness levels are relative to the linear actuator displacement from 0 mm (stiffness level 1) to 10 mm (stiffness level 6) by 2 mm rises. 36

3.10 Information gain for the different speeds 36

3.11 Information gain (K-L divergence) with stiffness levels and the whisking speed at the base stiffness 5. Whisking speeds are 10 mm/s, 14 mm/s and 18 mm/s. Stiffness levels are relative to the linear actuator displacement from 0 mm (stiffness level 1) to 10 mm (stiffness level 6) by 2 mm rises. 37

4.1 Schematic diagram of the whisker follicle with a Hall effect sensor (HS), a Permanent magnet (PM), and a piezoelectric sensor (PS). The soft joint is represented by a torsion ($k_\theta = 200$N/rad) spring, a linear ($k_1 = 0.2$N/mm) spring at $x = L = 8$mm and a controllable stiffness spring (k_f) at $x = D = 13$mm. The applied force at the tip of the whisker is F. (x_0, y_0) is the model reference frame origin (shown with ($\times$) in the figure) 40

4.2 Simulated correlation between the induced piezoelectric sensor stress (σ_{PS}) and the Hall effect sensor flux (B_{H}) against the follicle stiffness for three different natural frequencies (ω_n) and $w_{\max} = 5$mm. Notice the different axes scales. . . . 42

4.3 Experimental Setup (A) Hardware Setup and Programmed Path: (a) Data acquisition system (DAQ); (b) XY linear stage; (c) variable stiffness multimodal whisker follicle (VS-MWF); (d) Sandpaper holder; Programmed Path is $p1$, $p2$, $p3$ and $p4$ (Data is recorded only when the Whisker shaft moves from $p1$ to $p2$). (B) VS-MWF probing against a sandpaper. 43

4.4 (a) Raw data of Hall effect sensor for different frequencies and stiffness, (b) Raw data of piezoelectric sensor for different frequencies and stiffness 44

4.5 Covariance of Piezoelectric and Hall effect sensor signals for different combinations of stiffness and frequency for free whisker (whisker not touching a surface) and follicle vibrations . Red and blue ellipses refer to trials 1 and 2, respectively. Axes ranges are not shown for clarity. x and y axes are normalized to respect the aspect ratio. The range of the axes are from -0.0210 to 0.0210 and from -0.0069 to 0.0069 respectively for x and y. The shape of the ellipsoids represents the Eigenvalues of the principal components of each covariance matrix. 47

4.6 FFT of Hall effect sensor data at follicle stiffness 0.2970N/mm, 0.3661N/mm, 0.8328N/mm and whisking speed 10mm/sec, 14mm/sec ,18mm/sec on 80, 2000 grit sandpapers. 48

4.7 FFT of Piezoelectric sensor data at follicle stiffness 0.2970N/mm, 0.3661N/mm, 0.8328N/mm and whisking speed 10mm/sec, 14mm/sec, 18mm/sec on 80, 2000 grit sandpapers. 49

4.8 NSED - Normalize Standardized Euclidean Distance of RMS values computed using equation (4.7). The smallest circle represent the rough sandpaper, and the largest circle represent the smoothest sandpaper. At a given speed, the Standardized Euclidean Distance of the RMS values used to compare between roughest sandpaper (80 grit) against all other sandpapers. The sandpaper grit values are 80, 240, 320, 400, 600, 800, 1000, 1200, 2000, 3000, 5000, 7000. 50

4.9 Angle dependent stiffness in the whisker follicle inspired by Ringwulst(RW). This is actuated by servo motor and it change the stiffness while rotating 51

4.10 Continuous wavelet transform on Hall-effect sensor raw data. Highest stiffness in between 0.5s to 1.5s. 52

4.11 Continuous wavelet transform on piezoelectric sensor raw data. Highest stiffness in between 0.5s to 1.5s 53

5.1 Scan QR code to watch experiment videos. 58

Chapter 1

Introduction

Tactile sensing is one of the most important and complex sensory systems for most living beings. In order to acquire tactile information and explore the environment, animals use a wide range of biological mechanisms and transduction techniques. Whiskers, or vibrissae are a form of mammalian hair, found on almost all mammals other than Homo Sapiens. For many mammals, and especially rodents, these whiskers are essential as a means of tactile sensing [2]. Whiskers differ from regular pelage hair in the several ways, as detailed by A.S Ahl [3]. The mammalian whisker follicle contains multiple sensory receptors strategically organised to capture tactile sensory stimuli of different frequencies via the vibrissal system [4]. There have been a number of attempts to develop robotic whiskers to perform texture classification tasks in the recent past. Inspired by the features of the biological whisker follicle, this research intends to develop novel soft robotic whisker follicles and deeper insights into the biological basis of tactile perception in the mammalian whisker follicle.

(a) (b)

Figure 1.1: Examples of Whiskered animals: a) The mouse has whisker grid of five rows on each side of the snout, each row containing five to nine whiskers ranging between 15 and 50 mm in length. These whiskers help them for survival such as finding food escaping from predators. b) The cat whisker help them guiding in a limited environment such as moving through small hole and locating their food.

1.1 Literature Review

In the animal world, most mammals have whiskers [5] [6] [7]. The whiskers are more like wiry hairs growing out of an animals face, forehead, and legs, also called vibrissae. Often dogs, cats, rats and seals use whiskers [8] to help them follow their prey and navigation [9] [10]. Animals need to be able to hunt and move at night when eyesight is limited. In addition, some animals have trouble seeing things even when the object is directly in front of their noses. That may be due to their long snouts, like cat's eyesight limits in the range of 30cm and they have to relay on whiskers for close proximity perception . Therefore, animals whisk [11, 12] against objects to find food, guide them, measure things such as its size and shape [13] and surface texture [14, 15, 16, 17], usually in conjunction with the movement of the head[18, 19]. Figure 1.1 shows the examples of whiskered animals. Cats use their whiskers to figure out whether they fit through a tight space and find their prey. Seals use their whiskers to detect water movement to find fish. Remarkably, rat whiskers help them to make mental maps [20] of their surrounding world [21] [22]. These whiskers are different from normal hairs and rooted in the skin with various biomechanical properties, including sensory nerve cells.

Figure 1.2 shows a brief history of the development of whisker sensors, and the earliest research on biological whiskers can be traced back to 1912 by Vincent, S.B. The earliest study to illustrate the whiskers ability is by Vincent that rats use its whiskers to navigate through a

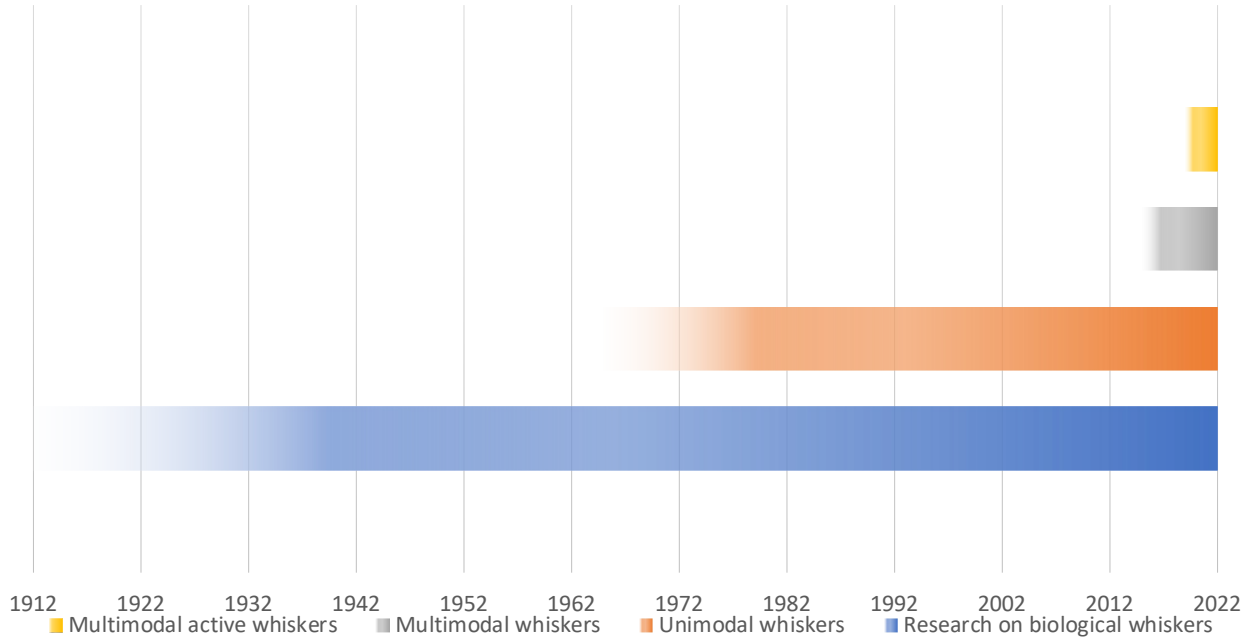

Figure 1.2: Visual representation showing a timeline of whisker base research evaluation in time .

raised labyrinth in 1912. This classic study, approaching its 110th anniversary, demonstrated for the first time the behavioral importance of whiskers: in maze navigation, rats became slow and prone to errors after whisker clipping.

1.1.1 Biological Description of the Whisker Follicle

Most research on whiskers has been done on the mystacial pad on rodents. The mystacial pad concerns the area directly under the nose, and comprises a highly uniform array of whiskers of varying length [23]. Whilst not all whiskers move, the mystacial pad of rodents is musculated, allowing the mammal hosts to 'whisker' - a motion of swaying the whiskers back and forth [24]. In rats, whisking happens at a dominant frequency of 8Hz [25]. Whilst intrinsic and extrinsic muscles allow 'whisking' to occur, the whole mystacial pad is also changeable in shape [24]. As a tactile sensor array, this means the mystacial pad is highly adaptable with several degrees of freedom.

In terms of anatomy, the whisker itself is not sensitive. Instead, all the transduction occurs

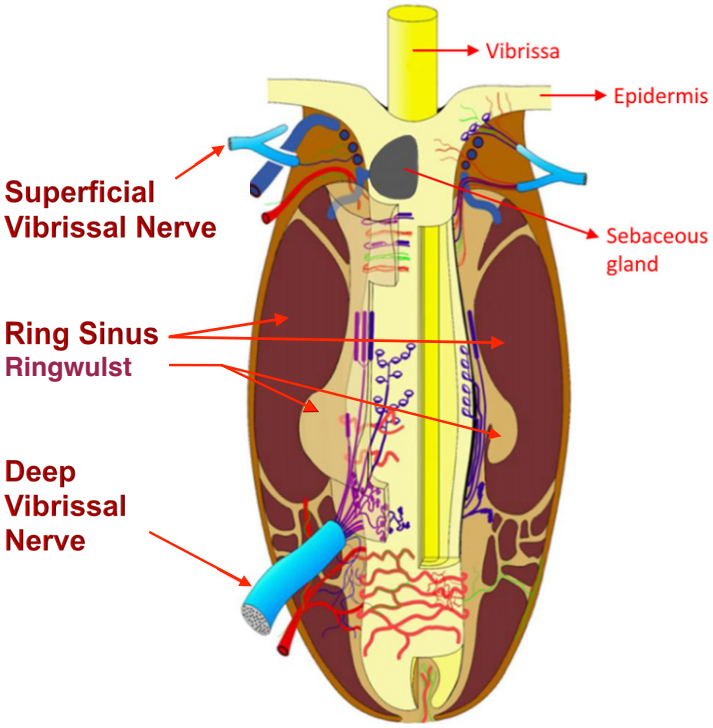

Figure 1.3: Anatomy of the rat whisker follicle (Diamond and Ehsan 2013).

at the follicle [26] [27] [28]. Figure 1.3 shows the anatomy of the rat whisker follicle. Each follicle has precisely one whisker, a rich blood supply, one or more sebaceous glands [3], and doughnut shape sing sinus with ringwulst. Again, unlike other hair follicles that use arrector pili, (involuntary muscles), the muscles attached to whiskers are striated, or voluntarily controlled. Moreover, each follicle is connected to a blood filled sinus, which each have a selection of different nerve receptors call superficial vibrissal nerve and deep vibrissal nerve. These nerve receptors include Pacinilike corpuscles, Merkel receptors, straight lanceolate terminals, branched circular lanceolate receptors, branched lanceolate endings, and endings of unmyelinated nerve fibers [3]. A single whisker sensor system may contain hundreds of these mechanoreceptors [29]. Indeed, the mechanoreceptors are known to encode information about small deflections, velocity, direction and amplitude of deflections [29].

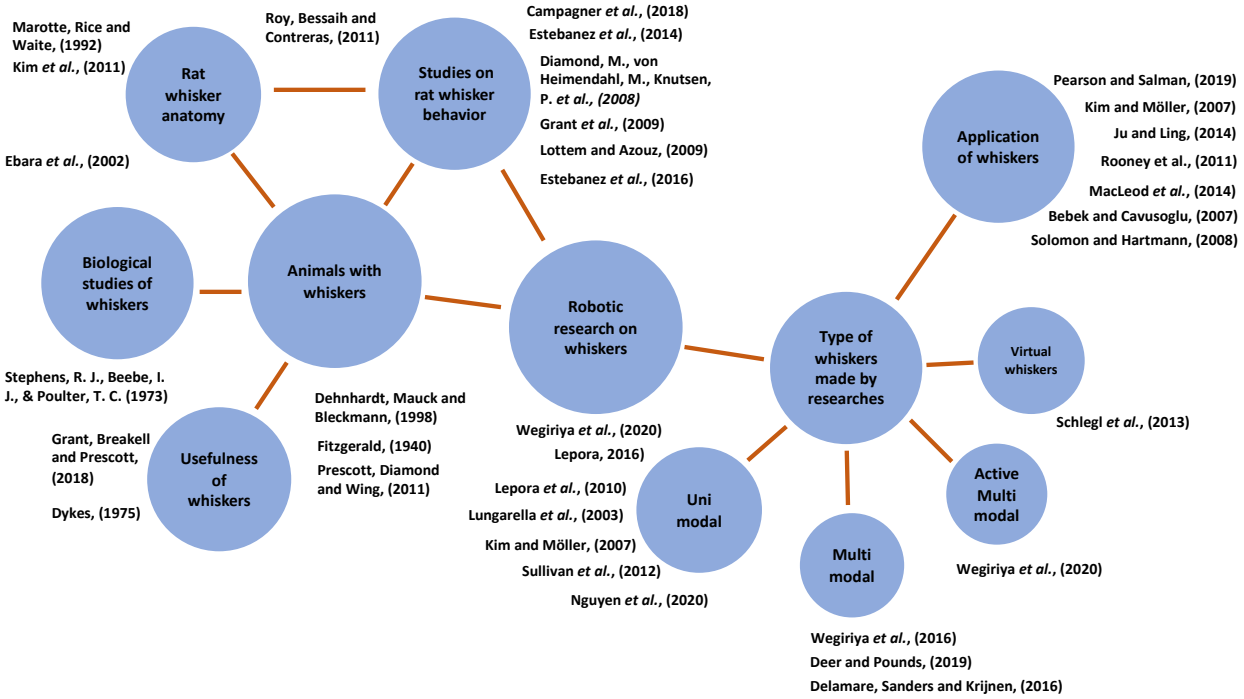

Figure 1.4: The layout map summarises the research development of whiskers.

1.1.2 Biological Inspiration for Artificial Whisker Sensors

Whiskers have been the focus of several works concerning artificial tactile sensors. Figure 1.4 shows the summarised map of the research development of whiskers. The map illustrates the inspiration from biology that leads to robotic research on whiskers [30] [31] [32]to the application of whiskers. Interestingly most of the studies developed Unimodal whiskers [33] [34][35], which uses a single sensor. In biology whiskers comprises multiple nerve receptors. However, research on multi-modal whisker sensors [36] [37] [38] is relatively low, which uses multi-sensors in a single body. In 1986, Hutson published a classic paper which presents a spatial task that can be performed without visual input and proves that rats require an intact pathway from one whisker to one cortical barrel in order to perform the task [39]. At the same time,unimodal whisker sensors are beginning to be installed on mobile robots for navigation and to avoid obstacles[40], to detect objects [41], shape recognition, and surface information [42].

Early whisker sensor designs, such as that of Russell [43][44], employ rigid whiskers as levers, with a means of measuring an angle change. Russell used a potentiometer - a resistive transducer - to determine the angle of deflection in his 2002 work. Most designs use simple trans-

duction techniques - the focus is instead on the mechanical properties of the whisker and array organisation.

As Russell notes, it is not always necessary to over-complicate the design with 'extra circuitry and wiring', if a series of simple devices are capable of achieving the same outcome [44]. For instance, a simple whisker attached to capacitor microphones has been able to discriminate between four different textures [45] with approximately a 70% success rate after only one sweep. Similar simple designs include that of Solomon and Hartmann, who used (piezoresistive) strain gauges to measure the deviation of four steel whiskers in two dimensions [46]. They used a novel technique that comprised of measuring the bending moment at the base of a whisker, in order to determine the point of contact along its length. By rotating the array around the object, they were able to correctly map the object in three dimensions [46][47][48]. Kim and Moller used the same technique, with Hall sensors instead of strain gauges [34] and authors of [49] developed miniaturised piezoelectric MEMS flow whiskers sensors.

Whilst these works illustrate that simple sensor designs can achieve good results, the designs themselves are much more focused on the direct sensing of objects and their properties, instead of *'the control of whiskers [whisking] and the impact of this control on sensing'*, as Pearson et al. state [47]. They focus their work on developing a whisking pattern with the aim of *'minimal impingement/maximal contact (MIMC)'* [47], meaning whiskers touch objects as often as possible, but with least force as possible.

The more recent 'ShrewBot' uses individually actuated whiskers, like in nature. These are based on the 'Biotact' sensor [50]. The Biotact sensor is inspired from biology in several aspects such as the vibrissal morphology, actuation and control of whiskers, and the vibrissal sensory processing. The sensory part of the Biotact sensor is, like Kim and Moller's work, a Hall Effect device, with a small permanent magnet [50]. Sullivan et al. concluded that '*the performance of both these approaches to classify textures after training on as few as one or two surface contacts was improved when the whisking motion was controlled using a sensory feedback mechanism*'. This shows, as Pearson et al. agree, that whilst the fundamental sensor has not changed, a distinct sensory advantage can be obtained when vibrissae are actuated

Table 1.1: A summary of published whisker tactile sensor

Application	Sensors	Advantages	Disadvantages	Reference
Obstacles Detection, and Location for navigation	Static Sensor	Single whisker detector installed on a hexapod robot as a simple binary proximity detector Bionic whisker in the front to determine whether there is an obstacle A simple tactile probe for surface identification and robot navigation combined with unsupervised learning	Passive detection Single detecting Point Local Navigation	Brooks Colin} P. Giguere
	Active Sensor	Active whisking tactile sensor array combined with the SLAM for robot navigation	Easily damaged	Salman
Objects Shape Detection and Recognition	Force-based sensor	Combining distance information and force directions to recognize objects' shape based on force-moment sensors Detecting the bend force direction of the antenna By rotating the whisker and collecting torque information to obtain the objects 3D information	Cannot provide efficient information to recognise the objects' shapes	Reference[14] Kaneko[15] Hartmann[17]
	Vibration-based Sensor	Measuring the contours of various 2D and 3D objects shapes by a vibration-based active antenna A tactile whisker array can reduce the pose dependence of object recall A whisker-like sensor installed on mobile robots can detect the nearby object's information both on land and underwater environments even measure external flow information		Hoinville[18] Pearson[19] Zhu[23]
Objects Texture Recognition and Classification	Bio-inspired whisker system	Different whisker systems were designed to collect vibration signals to recognize and classify different objects textures with high success, combing with naive Bayes or template method	Limited area of objects textures information	M.Fend[25] Evans[29] Sullivan[30]

intelligently.

1.1.3 Objects Shape Detection and Recognition

Vision-based methods have been the most popular approach to recognize [51]and classify [52]object material property because it is one of the most important properties of the surface of an object especially when a robot requires effectively interacting with its surrounding environment[53]. However, vision alone cannot estimate the objects physical parameters such as friction coefficients, roughness, and stiffness by itself. In this respect, artificial whiskers have been generally used as tactile (contact detection) sensors to recognize and classify the object's shape and material properties in extreme precision[54].

An active whisker was used to recognize the objects shape [55] information by combining distance information and force direction based on force-moment sensors [41], Kaneko[42] constructed an active antenna sensor to recognize the object's shape and determine the contact location by detecting the bend force direction of the antenna. However, these whiskers or antennas cannot provide efficient information to recognize the objects' shapes. Therefore, Russell proposed an idea that to use a tactile whisker to scan the objects surface to measure surface contours[56] . By rotating the whisker against a sequence of contact points of the object and collecting torque information, Solomon and Hartmann put forward a method to obtain the objects 3D information [57]. This idea was also utilised by Hoinville to design a vibration-based active antenna that has been validated by measuring the contours of various 2D and 3D ob-

jects shapes[58]. To enhance the efficiency of object recognition, Pearson developed a new pose control strategy for tactile whisker array which reduces the pose dependence of object recall when whisker slides the object surface[31] . More recently, the whisker-inspired tactile sensor system not only has been developed for object shape recognition in a static robot[54] but also mounted on mobile robot platforms working as an active exploration tool of the surrounding environment[59][60] . Rahn and Clements designed a novel tactile imager by mounting a flexible whisker on a mobile two-axis robot for object shape recognition[61]. A whisker-like sensor was constructed by Zhu for amphibious mobile robots to detect the nearby object's information both on land and underwater environments, as well as it can measure external flow information[62].

1.1.4 Texture Recognition and Classification of Objects

Object texture information is one of the most important properties and can be extracted by using a tactile sensor sweeping on the object surface. Artificial whisker sensors have been validated that it can work as an efficient tool to discriminate surface textures of target objects for robot[35][32]. A bio-inspired whisker system that includes capacitor microphones designed by M. Fend has been able to classify between four different objects textures with a high success rate with only a single sweep[63][64]. Later, H Hipp developed a novel artificial whisker to collect the vibration power spectrum and use it as a spectral classifier to classify objects textures [65]. This principle was also used by M. Evans to discriminate the raw floor texture vibration signal through a template matching algorithm, which is based on a whisker sensor system [66]. Moreover, Lepora employed the statistical properties of the whisker vibration signals to characterize textures by naive Bayes classifier, which is quite different from M. Evans method[30]. By pushing an active whisker sensor against different object surfaces, Sullivan achieved high-accuracy objects surface texture classification based on naive Bayes or template methods[67]. Lepora developed a biomimetic optical tactile whiskered robots for comparing the difference between fingertips and whiskers in[68]. Nguyen developed an artificial whisker system on both static and mobile platform with a novel object texture discrimination algorithm, the results of their experiments have shown that this system is efficient and robust[69].

Furthermore, Steigenberger theoretically analysed the connection between the object's surface texture properties and mechanical reactions of the vibration signals[70], and Bounce proposed an amplitude modulation/demodulation method for whisker-based texture recognition[71].

1.1.5 Obstacles Detection, and Location for navigation

Artificial Whiskers have been demonstrated in several studies that are a particularly high-efficiency method for animals such as rats and sea lions which can use them to navigate in dark and extreme environmental information and features without vision [72]. In 1989, Brooks installed the whisker detector on a hexapod robot as a simple binary proximity detector to assist navigation and obstacle avoidance [40]. Authors in [73] used capacitive sensing to demonstrate virtual whiskers for obstacle detection. The space robot Attila designed by Colin is equipped with a bionic whisker in the front to determine whether there is an obstacle. The bionic tentacle however, can only be used as a passive detector instead of actively detecting the size and distance of the obstacle [74]. It is hard to obtain terrain truth for the robots only using vision perception[75]. Then, M. Fend has used whiskers as contact detective sensors to avoid environmental obstacles during robot navigation [72]. A novel biomimetic whisker is constructed by Zhao to determine the location and distance of obstacles [76]. N. Cowan constructed the whiskers which have been used to perform wall following [77]. In[78] , Zurek showed that static whisker can act as locomotory guides that compensate for visual motion during fast locomotion P. Giguere and G. Dudek designed a simple tactile probe for surface identification and robot navigation combined with unsupervised learning [79]. In [80], an active whisking tactile sensor array has been successfully designed by Salman and combined it with the Rat-SLAM for robot navigation. Batlle designed a flexible whisker sensor with two degrees of freedom which can detect nearby objects by the sensing antenna beam and realize simple robot navigation[81]. In the last few decades, tactile sensors were applied to compensate for the vision limitation when in darkness, or underground, the application includes obstacle detection[82], underwater observation [83], object recognition [31] [84], object classfication[85], and manipulation[86],remotely deployable aerial inspection using tactile sensors [87]. Authors in [88] propose whisker sensor

design for robotic assisted beating heart surgery.

The several examples discussed here all employ previously existing technologies (sensors) in order to transduce the sensory information. In most literature, the focus is upon sensing modalities and not on the design of the whisker itself. There is therefore scope to investigate aspects such as optimal curvature, length and the material of whiskers. Furthermore, as Pearson et al. state, the motion of whisking is another important feature that should be considered in whisker-based sensors. This thesis details a whisker sensor that relies on whisking motions in order to identify different textures, through the application of multiple sensors.

1.2 Research questions

The aim of this research is to identify the biological features of the whisker mechanism and to mimic active perception in a robotic whisker sensory system.

1. **What are the morphological features of biological whiskers?**
   What mechanical properties of the whisker protruding outside flesh?

   What happens inside the flesh at the root of the whisker?

2. **What is the receptor interface mechanism of biological whisker?**
   What kind of biological mechanisms are there to capture flesh vibrations in response to whisker movement?

3. **How to setup a robotic whisker system considering the biological mechanisms?**
   What type of sensors are useful to capture tactile signals?

   What will be the best sensory system for active perception?

1.3 Research Contributions

The most important contribution is the design and use a novel soft whisker follicle comprising of two different frequency-dependent data capturing modules to derive deeper insights into the biological basis of tactile perception in the mammalian whisker follicle. In the design, the innervations at the Outer Conical Body (OCB) of a biological follicle are realised by a piezoelectric transducer for capturing high frequency components; whereas the innervations around the hair Papilla are represented by a hall sensor to capture low frequency components during the interaction with the environment. This research show how low dimensional information such as the principle components of co-variation of these two sensory modalities vary for different speeds and indentations of brushing the whisker against a surface. The novel variable stiffness multi-modal whisker sensor experimental results show for the first time that a multi-modal sensor can help to move the bandwidth of signal gain from low to high frequency information of textures by changing the stiffness and whisking speed. In particular, the findings show that the efficacy of robotic whiskers can be improved by using multi-modal transduction embedded in a controllable stiffness follicle, whereby the vibration dynamics of the follicle can be used to induce mutual information that the sensors cannot acquire in isolation. These new insights into the biological basis of tactile perception using whiskers provides new design guidelines to develop efficient robotic whiskers.

1.4 Publications

1.4.1 Conference Papers

Wegiriya H, Sornkarn N, Bedford H, Nanayakkara T. A biologically inspired multimodal whisker follicle. In2016 IEEE International Conference on Systems, Man, and Cybernetics (SMC) 2016 Oct 9.

Nanayakkara VK, Sornkaran N, Wegiriya H, Vitzilaios N, Venetsanos D, Rojas N, Sahinkaya MN, Nanayakkara T. A method to estimate the oblique arch folding axis for thumb assistive

devices. InAnnual Conference Towards Autonomous Robotic Systems 2019 Jul.

1.4.2 Journal Papers

Wegiriya H, Herzig N, Abad SA, Sadati SH, Nanayakkara T. A Stiffness Controllable Multimodal Whisker Sensor Follicle for Texture Comparison. IEEE Sensors Journal. 2019 Nov.

Akhond S, Herzig N, Wegiriya H, Nanayakkara T. A method to guide local physical adaptations in a robot based on phase portraits. IEEE Access. 2019 Jun.

Chapter 2

Multimodal Whisker Follicle

Nature comprises animals that are fully adapted to their environment. Nevertheless, we have noticed that whiskered mammalians are able to use their whiskers for their survival in nature,such as finding food, navigation and object recognition. However, nature has lots of whiskered animals that share similar features such as number of whiskers, orientation of the whiskers, and nerve types in the whisker follicle. In order to select the biological inspiration studies carried out searching for the mammalians that lives in under ground and has good sense of the surrounding environment. As a result, the rat was chosen due to advantages such as availability of detailed studies about the biology of rat whisker follicles and their capabilities of recognising surface properties.

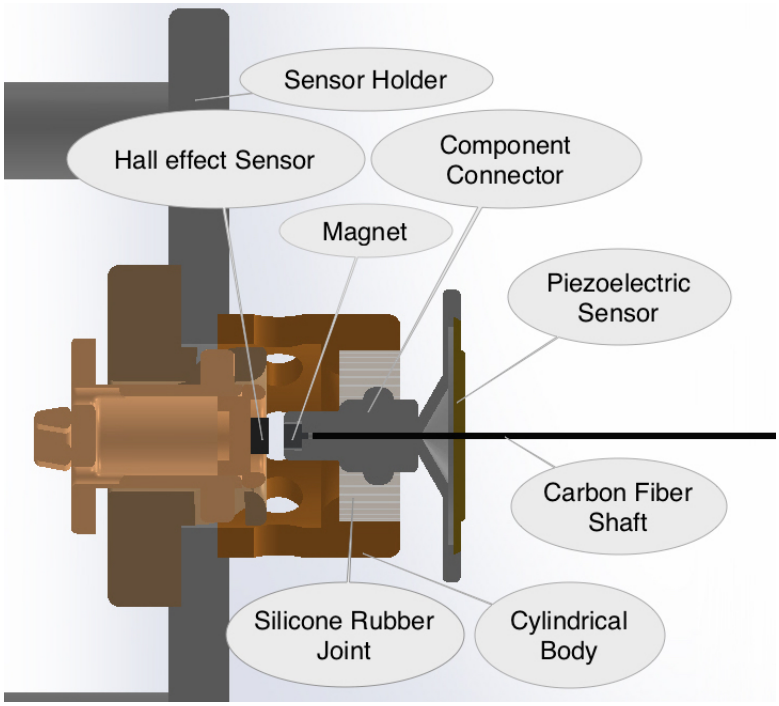

Figure 2.1: Constructed Whisker Sensor. The hall sensor is mounted inside the cylindrical body. The back end of the carbon fiber shaft is attached to a component connector through the piezoelectric sensor which holds the permanent magnet. The distance between the hall sensor and the permanent magnet was optimized based on the flux induced by the magnet.

2.1 Sensor Design

The whisker sensor shown in Figure 2.1 comprises a carbon fiber shaft embedded into a 3D printed cylindrical cantilever. The carbon-fiber shaft and 3D printed cylindrical cantilever are connected via a soft silicon rubber (Ecoflex 00-10) joint. The carbon fiber shaft, diameter 0.5mm and total length 200mm, passes through the drilled hole of the piezoelectric sensor. It is attached to a magnet holder, containing a magnet of diameter 2 mm. The linear hall effect sensor (Honeywell SS49E) is mounted at the base of 3D printed cylinder and linear to carbon fiber shaft (Whisker shaft). The whisker shaft is directly connected to the center of the piezoelectric sensor and placed on the magnet holder at a distance of 4 mm from the cylindrical body. Both sensors are connected to an analog to digital (AD) converter to measure their voltages.

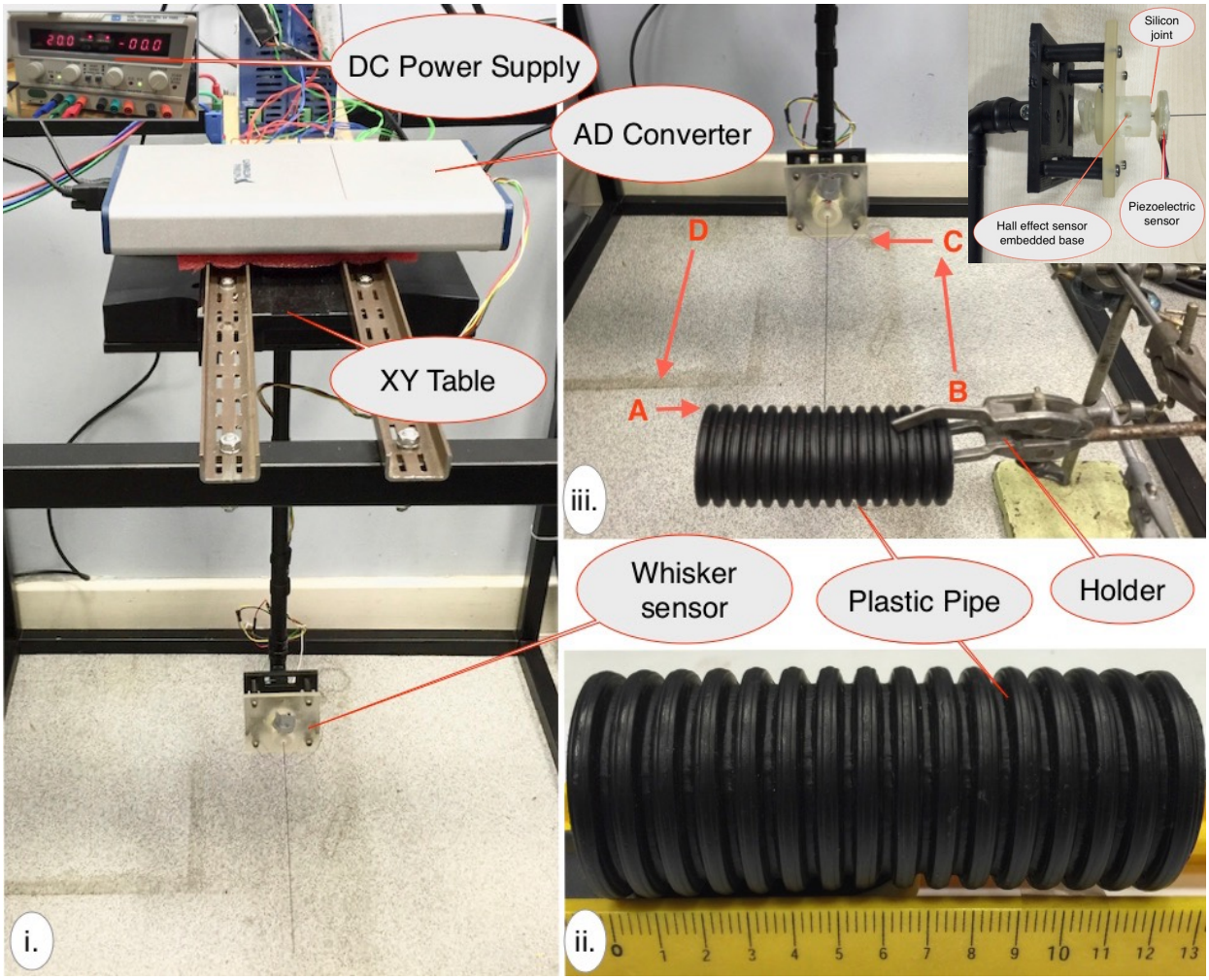

Figure 2.2: Experimental Setup, (i.) Hardware Setup, (ii.) Plastic Pipe, (iii.) Programmed Path - ABCD (Data recording starts when the Whisker shaft moving from A position to B, then data recording stops and sensor goes on the B,C,D route. When the sensor moving from D to A, program select the contact indentation and selected indentation added to D to A distance, then proceed on the square path.)

2.1.1 Characterisation of the Sensor

The sensitivity of the sensors depends on the vibration of the whisker shaft. When external vibrations are applied to the whisker shaft, the shaft deforms, and in turn, induces similar vibrations on the piezoelectric sensor. The vibrations displaces the magnet inside, causing a change in magnetic flux near the hall effect sensor. This effect generates high-frequency electrical signals from the piezoelectric sensor and low frequency signals from the hall effect sensor.

2.1.2 Experimental Setup

The experimental setup is shown in figure 2.2. The whisker sensor is horizontally attached to a rigid L-shape arm made with copper pipe and 3D printed ABS plastic.

The longer side of the arm is vertically mounted to the liner stage of an XY table (Aerotech-ANT130-160-XY-25DU-XY-CMS LOWER) to allow the whisker sensor to move in x and y directions. This linear stage is capable of moving up to 50mm/s. The whisker sensor signals are sent to a National Instrument NI USB-6341 analog to digital converter. The corresponding sampling rate of the AD converter is 1000Hz. In order to control the AD converter and XY linear stages, the set-up is connected to a computer with LabView2012, a National Instruments Corp. software. The Lab-view software synchronizes data retrieval and the liner stage motion. Data is then processed using MatLab R2013b, Mathworks Inc. software, which runs on an Intel Core i5 2.3GHz (64 bit) computer with 4 GB (RAM) of internal memory.

2.1.3 Experiment Process

In the experiment, the whisker is programmed to probe along the ripple side of a textured object sample. Here, use a plastic pipe with uniform and constant ripple throughout the surface (see Figure 2.2(ii)). The plastic pipe sample is fixed to the external holder and placed perpendicular to the whisker shaft (figure 2.2(iii)). The whisker sensor comes into contact with the surface of the material, by following the path shown in figure 2.2(iii). The contact indentation of the whisker shaft is controlled through a component parallel to the x-axis, and contact velocity through a component along the y-axis. Both of these movements are controlled through usage of the XY table. In this experiment, use 0 mm, 1mm, 2 mm, 3 mm, 4 mm, 5 mm indentation levels and 20 mm/sec, 15 mm/sec, 10 mm/sec, 5 mm/sec, 2 mm/sec contact speeds. Initially the indentation is set to 0mm, which provides a 'smooth touch' between the whisker and surface of the material. The corresponding contact speed of the whisker sensor is set to 20 mm/s. In a set of trials, the whisker successfully moved the programmed stroke length, and returned to its initial position via the programmed path. For each combination of indentations and contact

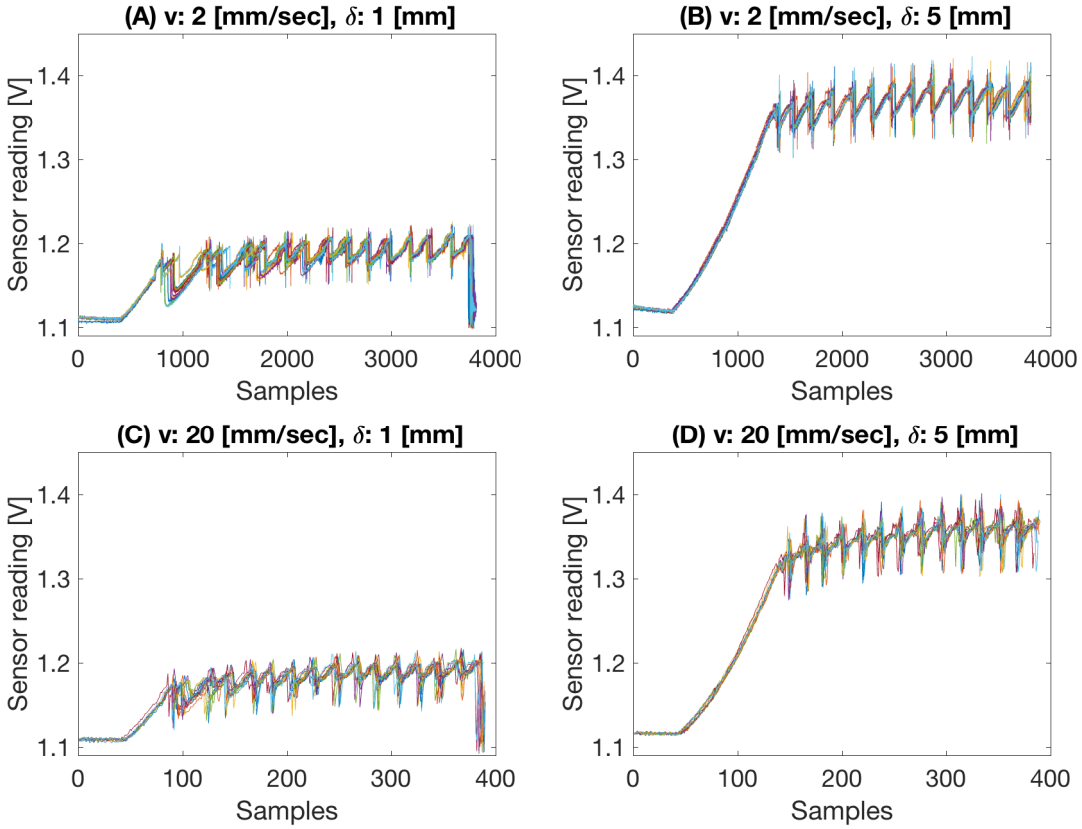

Figure 2.3: Hall sensor readings for two speeds and two indentation levels of brushing the whisker against the object in a constant distance shown in figure 2.2. The experiments were conducted for 5 speeds and 6 indentation levels. The plots show data from 20 trials for each speed-indentation combination. The plot C and D samples ten times less due to the speed.

speeds, collected data for 20 trials. Each trial contains 120 data samples. Therefore, for a given speed of contact, the five indentation levels gave 600 samples.

2.2 Results

Figure 2.3 shows hall sensor data for speeds, $v = 2$ and 20 mm/sec and indentation levels, $\delta = 1$ and 5 mm out of $v = 2, 5, 10, 15$, and 20 mm/sec, and indentations $\delta = 0, 1, 2, 3, 4$, and 5 mm. It can be observed that the increase in δ causes an increase in the magnitude of readings in the hall sensor (Figure 2.3 (B) and (D)). Since the magnitude of hall sensor readings depends on the magnitude of relative movements between the hall sensor and the permanent magnet, this indicates that higher indentation level causes higher amplitudes of vibrations at the bottom

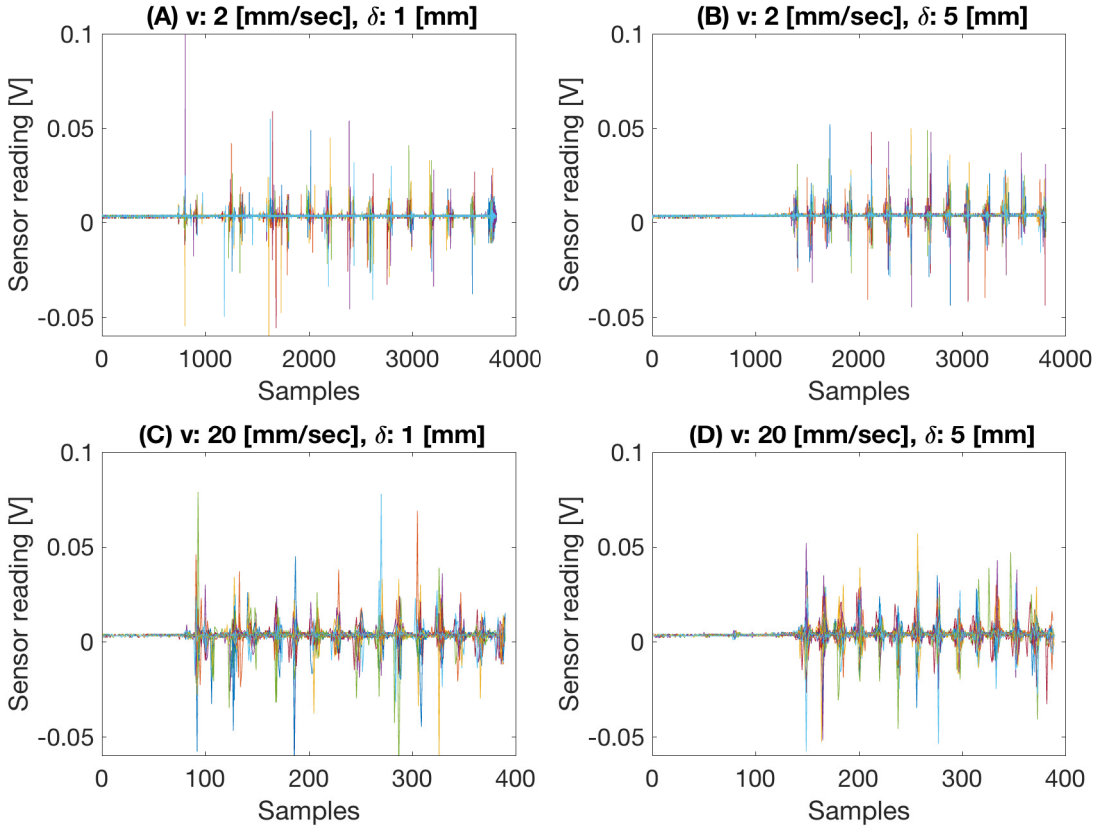

Figure 2.4: Piezoelectric sensor readings for two speeds and two indentation levels of brushing the whisker against the object in a constant distance shown in figure 2.2. The plots show data from 20 trials for each speed-indentation combination.The plot C and D samples ten times less due to the speed.

end of the whisker.

Figure 2.4 shows piezoelectric sensor data for speeds, $v = 2$ and 20 mm/sec and indentation levels, $\delta = 1$ and 5 mm. Unlike the hall sensor, can notice that higher indentations cause relatively lower peak amplitudes in piezoelectric sensor readings (Figure 2.4 (B) and (D)). Apparently, this figure also shows that higher speeds give higher frequencies of vibrations (Figure 2.4 (C) and (D)). Since piezoelectric transducers give readings proportional to the stress exerted on them, this implies that higher indentations cause lower stresses on the pivot point at which the piezoelectric transducer is mounted.

The co-variance of the readings of these two sensors across different speeds and indentation levels for multiple trials. Figure 2.5 illustrates the scatter plot for co-variation of readings given different speeds of brushing on the object shown in figure 2.2. Notice that the spread

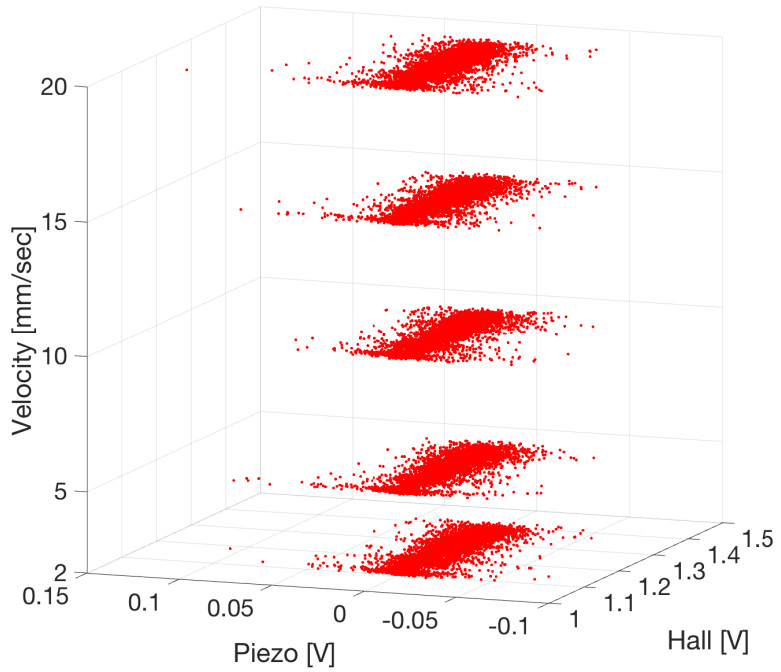

Figure 2.5: The co-variation of hall sensor and piezosensor data across 5 speeds for all 6 indentation levels.

of the distributions increase with increasing speed of brushing though the average values do not change significantly. This observations raises to question as to whether the direction of the principle components (eigen vectors of the co-variance matrix) gives higher variability when the speed of brushing increases.

Figure 2.7 shows the scatter plot for co-variation of readings given different indentations of brushing on the object shown in Figure 2.2. Notice that the major axis of the distribution rotates toward the hall sensor axis with higher indentations. This implies that the most significant principal component (the eigen vector of the co-variance matrix with largest eigenvalue) rotates from the piezosensor axis to the hall sensor axis when the indentation increases.

As observed in Figure 2.5, 2.6 and 2.7, the changes in the behavioural variables of the whisker could lead to the change in the geometrical properties of the correlation of the sensors' responses. These provide valuable insights into possible methods for information gain about an object by varying the speed and indentation of brushing the whisker with a follicle design proposed in this chapter.

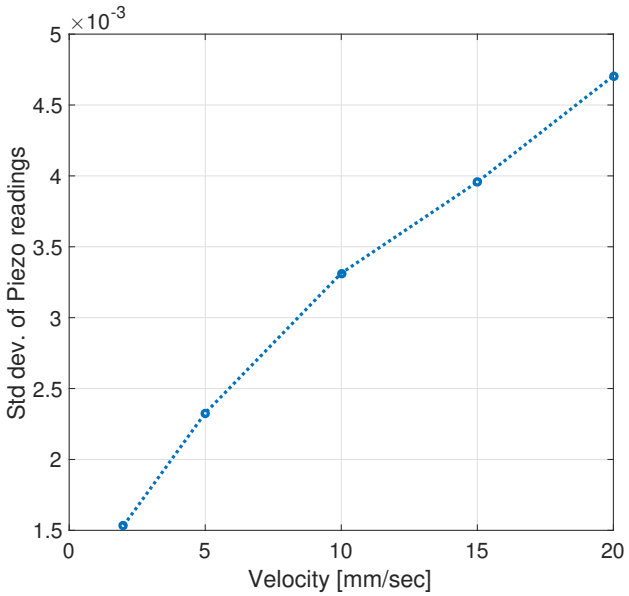

Figure 2.6: The stranded deviation of piezosensor data across 5 speeds for all 6 indentation levels.

As a result of probing behavioral changes (speed and indentation), further analysed the relationship between the co-variation of sensor readings. The eigenvectors and eigenvalues of the co-variance matrix, for the hall and piezoelectric sensors, were obtained for each reading. Figure 2.8 shows the behavior of the maximum eigenvalue and the angle of the corresponding eigenvector across indentation levels for all speeds of brushing. Notice that the maximum eigenvalue increases and settles down at a stable value when the indentation increases as shown in Figure 2.8(A). The angle of the eigenvector with the highest eigenvalue too settles down in a stable region as shown in Figure 2.8(B). Figure 2.8(C) shows that the standard deviation of the variability of the maximum eigenvalue increases and then decreases with the increasing indentation. Figure 2.8(D) shows that standard deviation of the angle of the eigenvector corresponding to the maximum eigen value converges to a stable region with increasing indentation levels.

If the conditional probability distribution of the maximum eigenvalue is given by $p(\lambda|\delta, v)$, where λ is the value of the maximum eigen value, the transfer entropy is given by

$$G = \sum_{\forall v \in \Re} p(\lambda|\delta, v) \log |\frac{p(\lambda|\delta, v)}{p(\lambda|\delta_0, v)}| \tag{2.1}$$

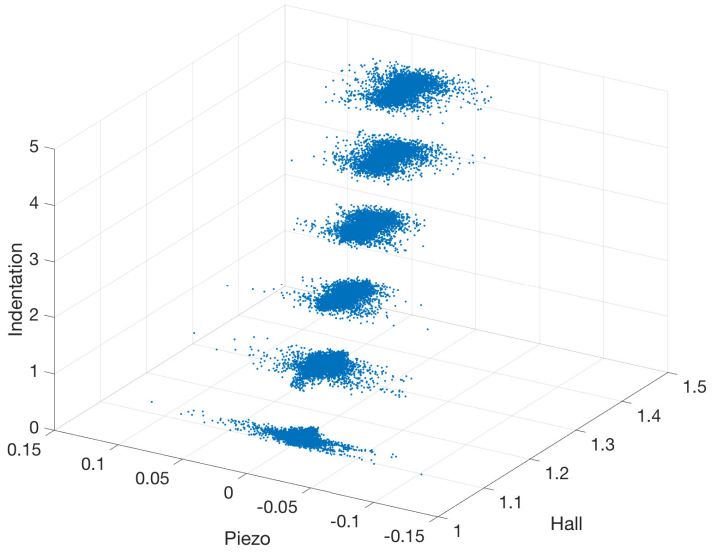

Figure 2.7: The co-variation of hall sensor and piezosensor data across 6 indentation levels for all 5 speed levels.

where δ_0 is the initial indentation, v is the speed of brushing the whisker on the object, and δ is the indentation. According to equation 2.1, a decrease in the width of $p(\lambda|\delta, v)$ would result in a drop and settling down of the the transfer entropy, G (a measure of the information gained by varying the indentation across all speeds), as shown in Figure 2.9. This implies that indentations higher than a certain range is not going to yield more information.

Figure 2.8 also shows that higher speeds of brushing the whisker shows highest sensitivity to changes in indentation. For instance, in figures Figure 2.8(B) and (C), the curve corresponding to speed-4 shows the highest rate of change.

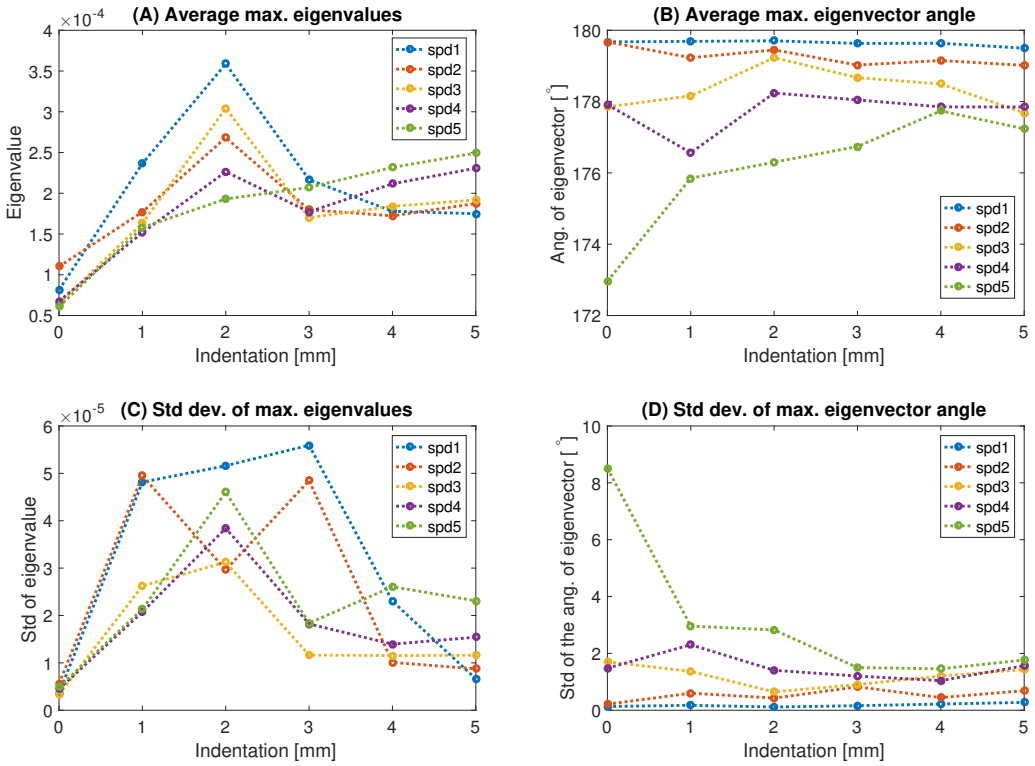

Figure 2.8: Average behavior of maximum eigenvalues of the covariance matrix for hall sensor and piezosensor readings across different indentation levels and speeds of brushing the whisker.

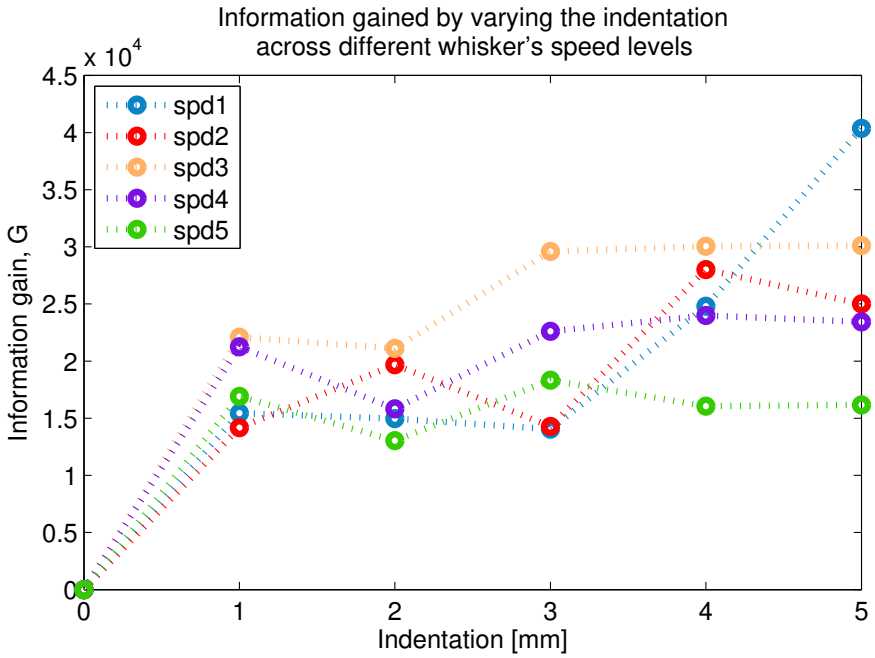

Figure 2.9: The transfer entropy measured by the information gained during the variation of indentation levels across different whisker's speed levels

Chapter 3

Stiffness Controllable Multimodal Whisker Follicle

In the animal world surviving from predators has to be very fast. The nocturnal species have this vital capability even in low visibility environments. That capability of these animals may come from the special tissue dynamics helping the brain to do the quick and efficient signal processing. Therefore, the whisker follicle can reduce the computing process and optimize the filtering of tactile signals. Inspired by the features of biological whisker follicle this chapter explains the design and use of a stiffness controllable soft whisker follicle comprising of two different frequency-dependent data capturing modules to derive deeper insights into the biological basis of tactile perception in the mammalian whisker follicle.

3.1 Introduction of the Stiffness Controllable Whisker Follicle

Whiskers are innervated by multiple mechanoreceptors [89] [90]. The follicle sinus complex (FSC) amplifies the vibrations of the whisker allowing the mechanoreceptors at the base to capture extremely small stimuli [91] [27]. Authors of [92] used psychophysical methods to investigate, how fixed head mice can localize an object along the axis of a single whisker and the stresses at the follicle relative to the stiffness of the whisker shaft.

Although works in the chapter one explain that a simple sensor setup can obtain good results, further work is needed to explore the potential of the whisker follicle dynamics to improve information [93]. The 'Biotact' sensor for classifying the surface textures is a recent advancement in this direction [50]. This bio-inspired sensor has the ability of actuation and control of the whisker, and the sensory part contains a small permanent magnet and hall effect device [50]. Additionally, [94] shows that robotic whiskers could be used for high fidelity tactile exploration for distinguishing object shapes and contours.

These examples focus on sensing modalities in order to capture sensory information and not on the design of the whisker follicle itself. Therefore, there is scope to investigate features such as an effect of stiffness control at the follicle level, the optimal range of stiffness and speed of whisking to maximize information gain.

This chapter demonstrates that multi-modal whisker sensing with variable stiffness and whisking motions have a major effect in order to distinguish lookalike textures. Moreover, in the design shown in Fig. 3.1 represent deep vibrissal nerves by a hall effect sensor and superficial vibrissal nerves by a piezoelectric sensor, and the stiffness controllable mechanism represents the possible function of the ring sinus. Furthermore, it shows that how gain response and low dimensional information such as the principal components of co-variation of two sensory modalities vary for different frequencies and stiffness brushing the whisker against a surface. This study allows us to take a robotic approach to provide insights into the biological function of the above arrangements in a rat whisker follicle.

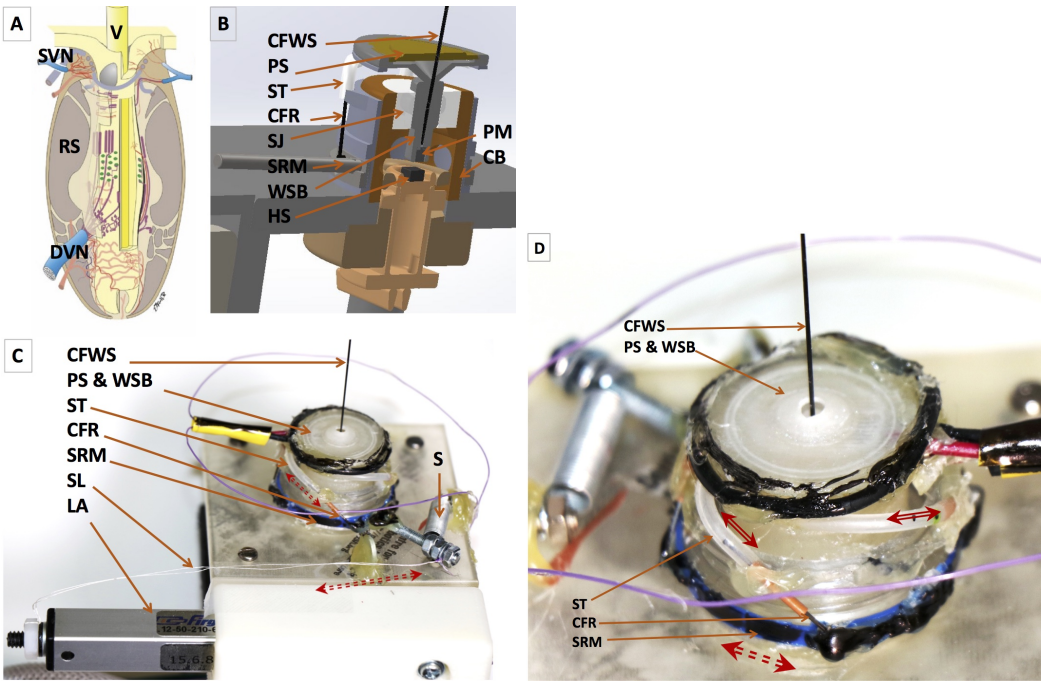

Figure 3.1: Whisker follicle. (A) Schematic illustration of the structure innervation of a rat whisker follicle [1]; V, vibrissal shaft; RS, ring sinus; SVN, superficial vibrissal nerve; DVN, deep vibrissal nerve. (B) Cross section of the variable stiffness multimodal whisker follicle (VS-MWF); CFWS, carbon fibre whisker shaft; PS, piezoelectric sensor; ST, silicone tube; CFR, carbon fibre rod (It has four); SJ, silicon joint; SRM, steering ring mechanism; WSB, whisker shaft base; HS, hall sensor; SL, string link; LA, linear actuator; PM, permanent magnate; CB, 3D printed Cylindrical body. (C) Complete VS-MWF; S, spring. The spring is used to relocate the SRM, when the LA is decreasing the actuated length. (D) Enlarged VS-MWF to demonstrate the stiffness controllable system.

3.2 Experimental Methodology

The variable stiffness multi-modal whisker follicle (VS-MWF) with two sensor modalities shown in Fig. 3.1 is an advancement from the constant stiffness multi-modal whisker follicle (CS-MWF) reported in [38]. The VS-MWF is comprised of a 3D printed cylindrical body (CB), a soft silicon rubber (Ecoflex 00-10) joint (SJ), a rigid 3D printed whisker shaft base (WSB) containing a 2 mm diameter permanent magnet (PM), a 0.5mm diameter 200mm long carbon fibre shaft (CFWS), a Hall sensor (HS), and a piezoelectric sensor (PS). The piezoelectric sensor is attached to the WSB. The carbon fibre shaft passes through the centre of the piezoelectric sensor and rests in the WSB which is free to move due to the silicon rubber medium around it. There is a gap of 4 mm between the cylindrical body and the piezosensor holder to allow the WSB to oscillate when the whisker vibrates.

The stiffness controllable system comprises four carbon fibre shafts (0.5 mm diameter and 17 mm length) sliding into four equally spaced silicon tubes (1 mm internal diameter, 2 mm outer diameter, and 24 mm length) attached to the top of the WSB. A steering ring mechanism was designed to control the carbon fibre shafts, so that all four carbon fibre shafts move into the silicon tubes when the ring rotates clockwise concentric to the WSB. The range of displacement of the carbon fibre shaft is from 0 to 3.2 mm in steps of 0.4 mm. In the rest of the paper, each step denotes a linear actuator pulling level where these levels are numbered from 1 to 9. The stiffness of the WSB joint increases when the carbon fibre shafts are moved into the silicon rubber tubes. The steering ring is controlled by a Linear actuator Actuonix L12-50-210-6-l. The signals of both sensors and the linear actuator are acquired and controlled through a data acquisition and control system, respectively.

3.2.1 Characterisation of the Sensor

The sensitivity of the sensors depends on the vibration of the whisker shaft and the stiffness of the silicone joint. When the whisker shaft vibrates, the shaft and silicon joint deforms, and in turn, stimulates similar vibrations on the piezoelectric sensor and the magnet inside. The displacement of the magnet attached to the bottom of the WSB triggers a fluctuation in magnetic flux around the hall effect sensor. This study results in high-frequency electrical signals in the piezoelectric sensor and low-frequency signals in the hall effect sensor mimicking the function of the superficial vibrissal nerve and the deep vibrissal nerve respectively. **The stiffness controllable silicone joint that mimics the ring sinus muscles in a biological whisker follicle can influence the sensor signals by changing the follicle vibration dynamics.**

3.2.2 Experiment Setup

The experimental setup is shown in Fig. 3.2. The whisker sensor is horizontally attached to a 3D printed ABS plastic holder. This holder is connected to a 36 cm L-shape rigid copper pipe

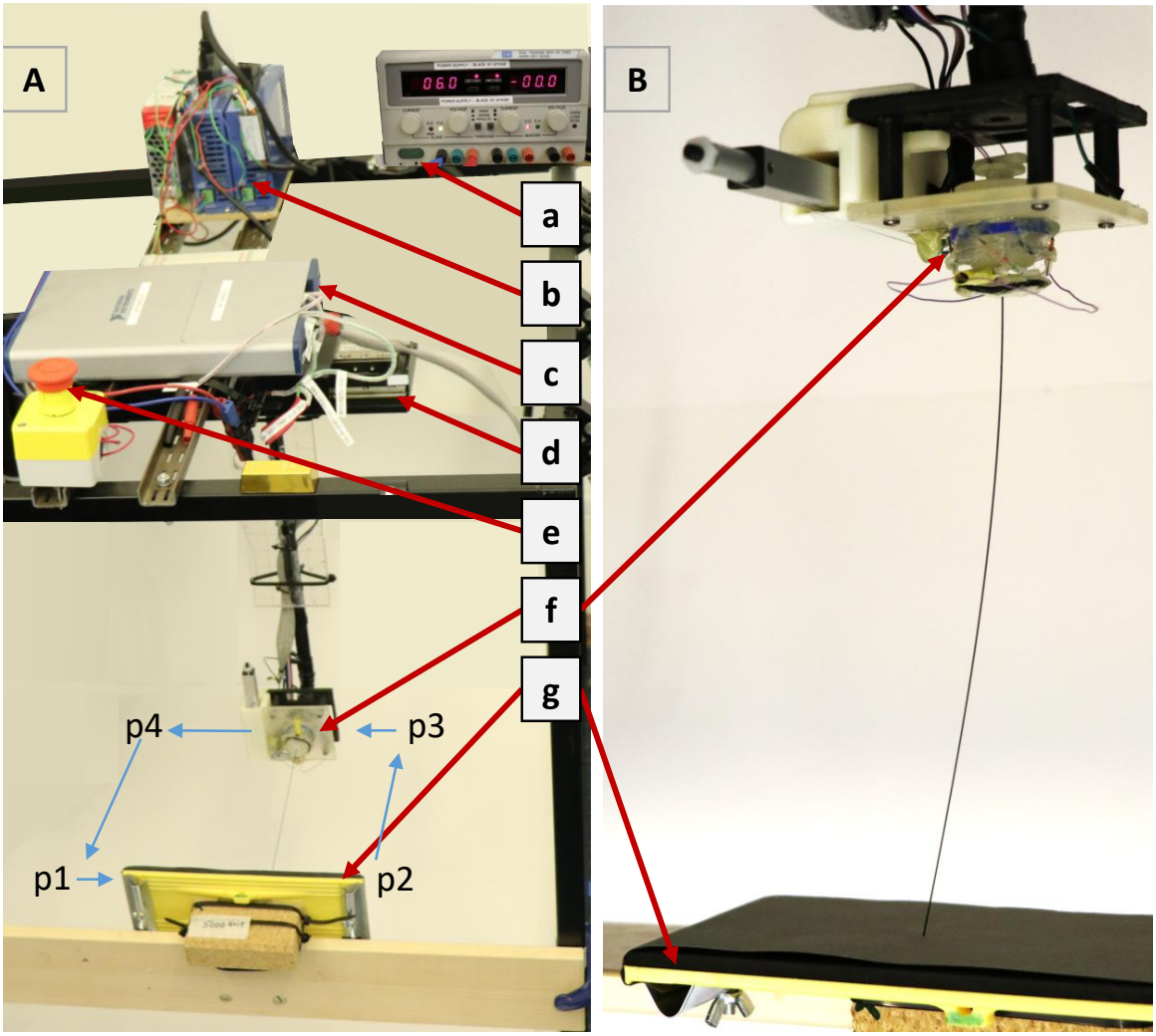

Figure 3.2: Experimental Setup, (A) Hardware Setup and Programmed Path; Hardware Setup - (a) Power supply (b) Controller of the XY linear stage, (c) Data acquisition (DAQ), (d) XY linear stage (e) Emergency stop switch, (f) VS-MWF (g) Sandpaper holder, Programmed Path is $p1$,$p2$,$p3$ and $p4$ (Data recording starts when the Whisker shaft moving from $p1$ position to $p2$, then data recording stops and sensor goes on the $p2, p3, p4$ route), (B) variable stiffness multimodal whisker follicle (VS-MWF) probing against a sandpaper

arm whose longest side is strengthened using an acrylic sheet. The end corresponding to the longest side of this arm is attached to the XY stage (Aerotech- ANT130-160-XY-25DU-XY-CMS LOWER) through a 7 cm $\times$ 7 cm $\times$ 5 mm rigid 3D printed ABS plastic plate. This stage allows controlling the movement of the whisker sensor along the x and y directions.

A National Instrument NI USB-6341 Multifunction I/O Device together with a LabView2016 interface were used to acquire signals from the whisker sensor at 10kHz sampling rate and to control the RRM, and XY linear stage. MatLab R2016a, Mathworks Inc, was employed for the synchronization and analysis of the data.

3.2.3 Experiment Process

Experiment-1: Characterisation of the natural frequency of the VS-MWF

In the initial experiment, the whisker movements is programmed to vibrate 30 cycles each at 8 Hz to 23 Hz in 1 Hz steps (16 frequency steps in total)by XY table. The magnitude of oscillation along the y-axis of the X-Y stage was kept at 0.5mm. I trialled 0.2 mm, 0.5 mm and 0.8 mm oscillation magnitudes to choose the best option that gave a reasonable signal to noise ratio. I dropped 0.2 mm magnitude because the signal magnitudes was too low and 0.8 mm oscillation was also dropped because it vibrated the whole mounting making difficult to distinguish the signal due to the oscillations in the VS-MWF from other structural vibrations.

In this experiment I used 1 to 9 stiffness levels for each frequency. Initially, the stiffness is set to level 1 (carbon shafts inserted at the lowest level into the silicone tubes attached to the WSB joint), which provides a default stiffness of the silicon joint between the two sensors of the whisker follicle. The corresponding initial frequency of the whisker sensor is set to 8 Hz. In a set of trials, the whisker vibrates 30 cycles, then stops and stabilizes at its initial position. For each combination of stiffness levels and frequency levels acquired data for 2 trials of 30 cycles each.

Then I took the first 100 samples (10 ms) in each trial to compute the base level readings of both the hall and piezo sensors and subtracted this from the raw data to obtain signals that are caused due to the oscillations.

Experiment-2: Information gain in texture discrimination with VS-MWF

In the second experiment, the whisker is programmed to probe along the rough side of two similar featured material samples for 7.5 cm span. The whisker was moved to the edge of a sandpaper holder with an indention of 3 mm before starting to sweep across the sandpaper at different speeds. I chose a 3 mm indentation based on my previous results of information gain [38]. The 3 mm indentation was such that the whisker bent till the XY table moved for 19 mm

sideways before the tip of the whisker started to sweep the sandpaper.

Here, I use two sandpapers with 3000 and 5000 grit roughness respectively. In the experiment, one sandpaper sample is fixed to the external holder and clamped perpendicular to the whisker shaft (Fig. 3.2(i)). Initialisation of the experiment for each sandpaper sample is identical for all the iterations. By following the path shown in Fig. 3.2(i), the whisker sensor comes into contact with the surface of the sandpaper. These movements are controlled through the usage of the XY table and I used 1 to 6 stiffness levels for each contact velocity because the natural frequency characterisation in section 4.0.3 showed that best signal to noise ratios can be obtained within this stiffness range. The component parallel to the x axis controlled the contact indentation and the component along the y axis controlled the whisking velocity of the whisker shaft. In this experiment use 3 mm contact indentation across all iterations and 10 mm/s, 14 mm/s, 18 mm/s, whisking speeds. Initially, the stiffness is set to level 1, as the default stiffness of the silicone joint between the two sensors of the whisker follicle and the corresponding whisking speed of the whisker sensor is set to 10 mm/s. The whisker completely moved the programmed stroke length and returned to its initial position via the programmed path while maintaining the stiffness level at the given trial. For each combination of stiffness levels and contact speed, I acquired data for 2 trials. Therefore, for a given stiffness level, the three contact speeds gave 6 data sets for a single sandpaper.

I took base readings and subtracted data as described in the last paragraph of section 4.0.3. Moreover, I dropped the first 4 seconds of data to remove the data corresponding to the initial whisker - tested surface collision. The remaining hall and piezoelectric sensor data were divided into 200 bins to compute covariance between the two sensor modalities so that the two textures can be compared at a bin level. The bin level comparison was then used to construct a probability distribution of a texture difference metric. A sharpening or shifting of the probability distribution of the difference metric due to a change in follicle stiffness and whisking speed amounts to entropy reduction which was measured using Kullback-Leibler divergence (transfer entropy or information gain).

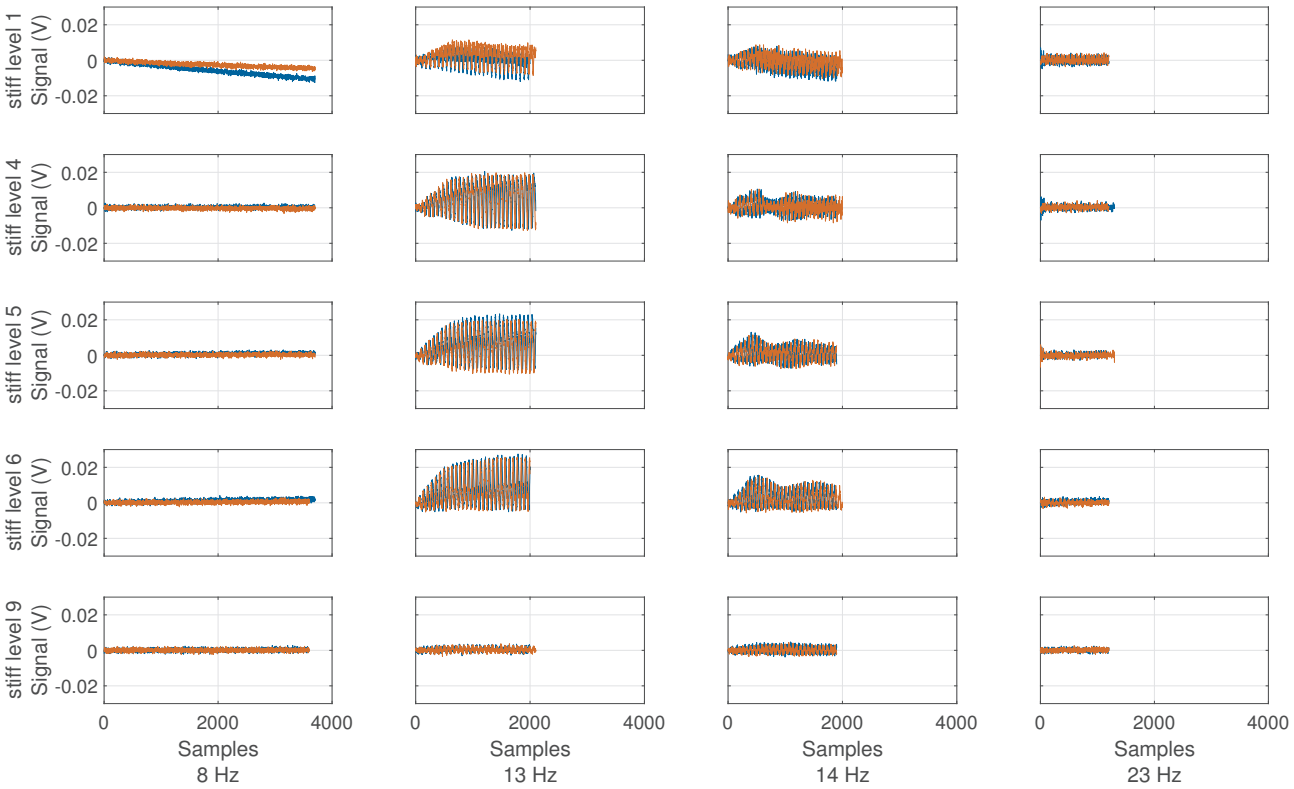

Figure 3.3: Raw data of Hall sensor for different frequencies and stiffness. The red line refers to the first trial, the blue line refers to the second trial.

3.3 Results

Fig. 3.3 and Fig. 3.4 shows the base subtracted raw experimental readings (see section 4.0.3 in the methods section for details) from the Hall sensor and the Piezo sensor mounted in the VS-MWF for selected levels of oscillation frequencies (8, 14, 15 and 23 Hz) and stiffness levels (1, 4, 5, 6 and 9). I can observe a higher magnitude of signals for 14-15Hz oscillation frequency. This can also see magnitude variation depending on the stiffness of the VS-MWF.

Then I looked at the root mean square (RMS) value of the signals to find more refined information of how the signal magnitudes depend on frequency and stiffness. Fig. 3.5 shows the hall sensor RMS values for frequencies 8 Hz to 23 Hz and stiffness levels 1 to 9. I noticed that RMS value reached its maximum in Fig. 3.5 around 14 Hz and Stiffness levels 3-6. This illustrates that the change in stiffness of the follicle amplifies the power of the signal at the bottom end of the whisker.

Fig. 3.6 shows that the piezoelectric sensor RMS values for frequencies 8 Hz to 23 Hz and

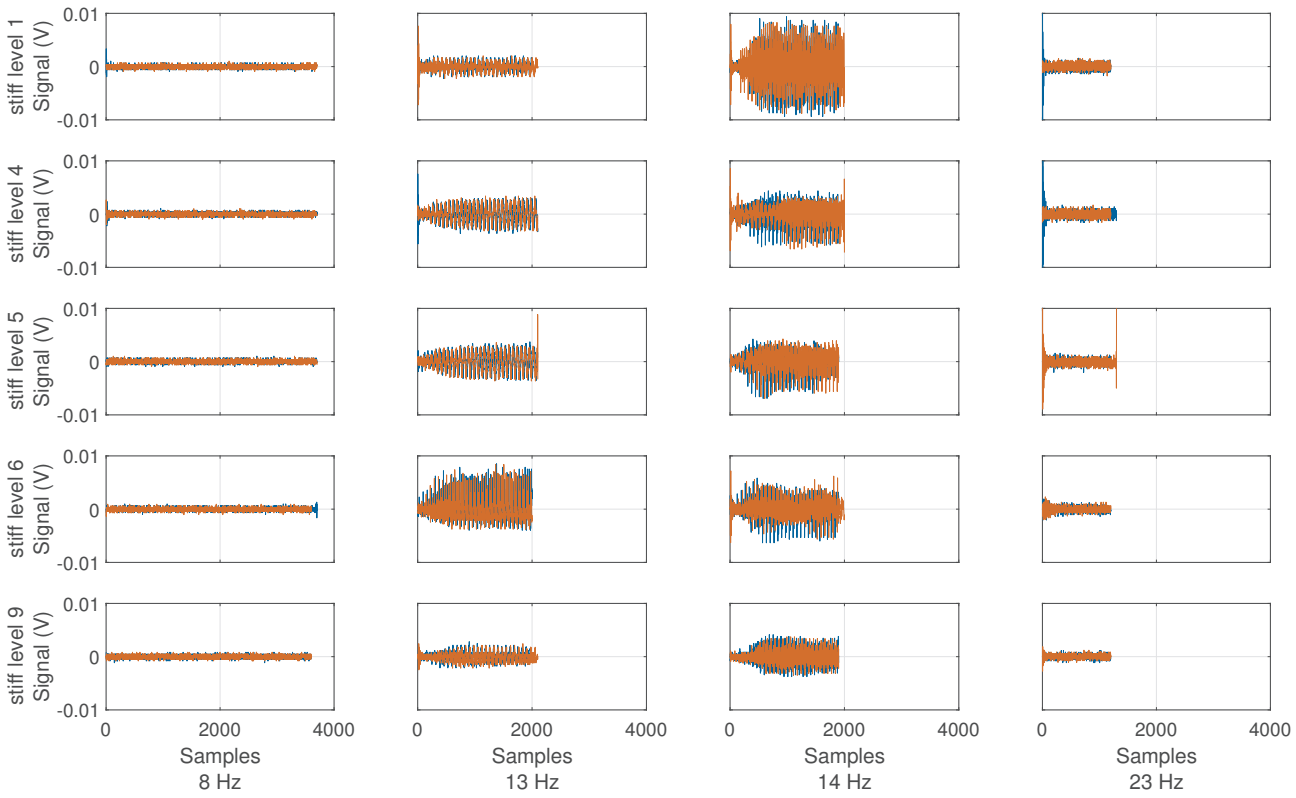

Figure 3.4: Raw data of piezo sensor for different frequencies and stiffness. The red line refers to the first trial, the blue line refers to the second trial.

stiffness levels 1 to 9. I notice that RMS value reaches its maximum in Fig. 3.6 around 14-15 Hz and Stiffness levels $1-6$.

The observations in Fig. 3.5 and Fig. 3.6 indicate a common dependency of signal magnitudes on the follicle stiffness and oscillation frequency. Then I looked at the co-variance of the hall and piezoelectric sensor readings across 8 Hz to 23 Hz and stiffness levels 1 to 9. Fig. 4.5 illustrates the ellipse plot for co-variation of readings. I can observe that certain resonance in the co-variance around oscillation frequency 14Hz and stiffness levels 3 - 6 in Fig. 4.5.

These results provide important clues to maximize information gain in texture classification by maximizing the signal to noise ratio of measurements. To demonstrate this effect, I did a second experiment that involves distinguishing two lookalike sand papers (3000 grit and 5000 grit) described in more detail in section 4.0.3 in the methods section.

Then for both sandpapers, I looked at the co-variance of the hall and piezoelectric sensor data in 200 bins across speeds 10, 14, 18 mm/s and stiffness levels 1 to 6. Fig. 3.8 illustrates the

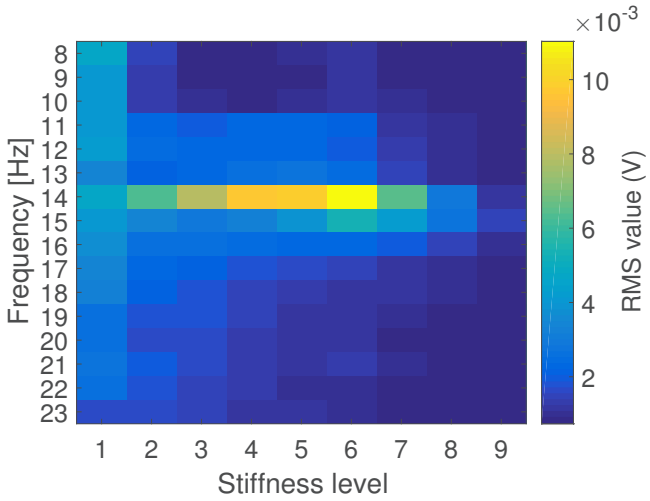

Figure 3.5: The colorbar represents the root mean square (RMS) of Hall sensor with stiffness level and frequency [Hz]. Stiffness levels are relative to the linear actuator displacement from 0 mm (stiffness level 1) to 16 mm (stiffness level 9) by 2 mm rises.

ellipse plot for co-variation in all bins. The red ellipses correspond to whisking against 3000 grit and the blue ellipses correspond to the 5000 grit sandpapers. This observation shows that the distance between two co-variance matrices changes with varying stiffness levels and speed. I quantify the difference of the co-variance matrices using the Frobenius distance given by

$$F_d = \sqrt{trace((\mathbf{A}-\mathbf{B})^T(\mathbf{A}-\mathbf{B})} \tag{3.1}$$

where, $\mathbf{A}$ is the covariance matrix of the two sensor modalities corresponding to the 3000 grit sandpaper data and $\mathbf{B}$ is corresponding to the 5000 grit sandpaper data.

Since F_d this only accounts for the difference between the covariance matrices that are computed after subtracting the expected values of the corresponding data, I define a new difference metric ζ by multiplying F_d by the euclidean distance $\|d\|$ of the expected values of the two sensor readings between two given textures in each bin given by

$$\zeta = \|d\| \, F_d \tag{3.2}$$

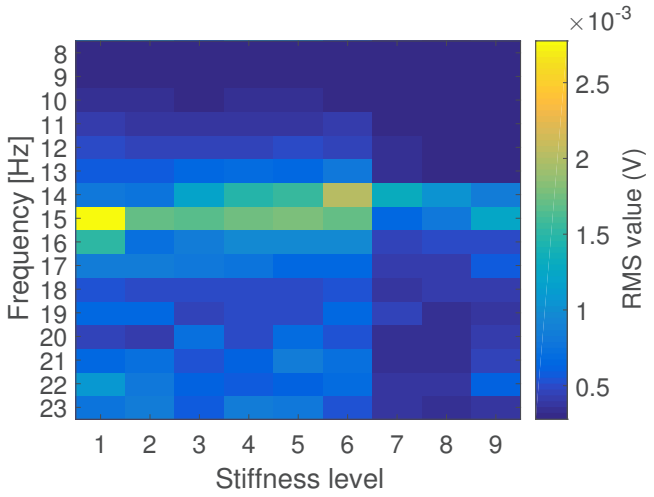

Figure 3.6: The colorbar represents the root mean square (RMS) of Piezo sensor with stiffness level and frequency [Hz]. Stiffness levels are relative to the linear actuator displacement from 0 mm (stiffness level 1) to 16 mm (stiffness level 9) by 2 mm rises.

where $\|d\| = \sqrt{d^T d}$ with

$$d = \begin{bmatrix} \bar{h}_i - \bar{h}_j \\ \bar{p}_i - \bar{p}_j \end{bmatrix} \tag{3.3}$$

where $\bar{h}_i$ and $\bar{h}_j$ are the expected values of the signals acquired by the hall sensor for materials i and j in a given bin respectively. $\bar{p}_i$ and $\bar{p}_j$ are the expected values of the signals acquired by the piezoelectric sensor data for materials i and j in a given bin respectively. In this particular case, i and j correspond to the 3000 and 5000 grit sandpaper respectively.

Then I looked at the probability distribution of ζdifferent whisking speeds and stiffness levels. Fig. 3.9 shows the results of this analysis for whisking speeds 10 mm/s, 14 mm/s and 18 mm/s with stiffness levels 2 and 5 out of all combinations for clarity. Here I can notice that at the speed of 14 mm/s and stiffness level 2 the probability distribution has a sharper peak compared to the stiffness level of 5 and other whisking speeds. This implies that the interaction effect of the speed of whisking with follicle stiffness help to gain information (maximize transfer entropy) in a texture classification task.

The quantify transfer entropy using the Kullback-Leibler divergence G given by

$$G = \sum_{\forall v \in \Re} P(\zeta|k, v) \log |\frac{P(\zeta|k, v)}{Q(\zeta|k_0, v)}| \tag{3.4}$$

Figure 3.7: Covariance of Piezoelectric and Hall sensor with stiffness and frequency. Red and blue ellipses refer to trials 1 and 2 respectively. Axis ranges are not shown for clarity. Both x and y axises range from -0.02 to 0.02

where, $P(\zeta|k, v)$ the probability distribution of the Frobenius distances x at an arbitrary stiffness level k, and whisking speed v, and $Q(\zeta|k_0, v)$ is that for the base stiffness level k_0.

According to the equation 3.4, sharpening or shifting of $P(\zeta|k, v)$ relative to $Q(\zeta|k_0, v)$ would yield higher information gain.

Fig. 3.10 shows the information gain analysis for all combination of follicle stiffness at different speeds. For clarity, Fig. 3.11 shows the information gain from stiffness level 5 to all the other stiffnesses for speeds 10, 14 and 18 mm/s. Here I observe that at speed 14 mm/s stiffness level 2 has the higher information gain compared to the base stiffness 5.

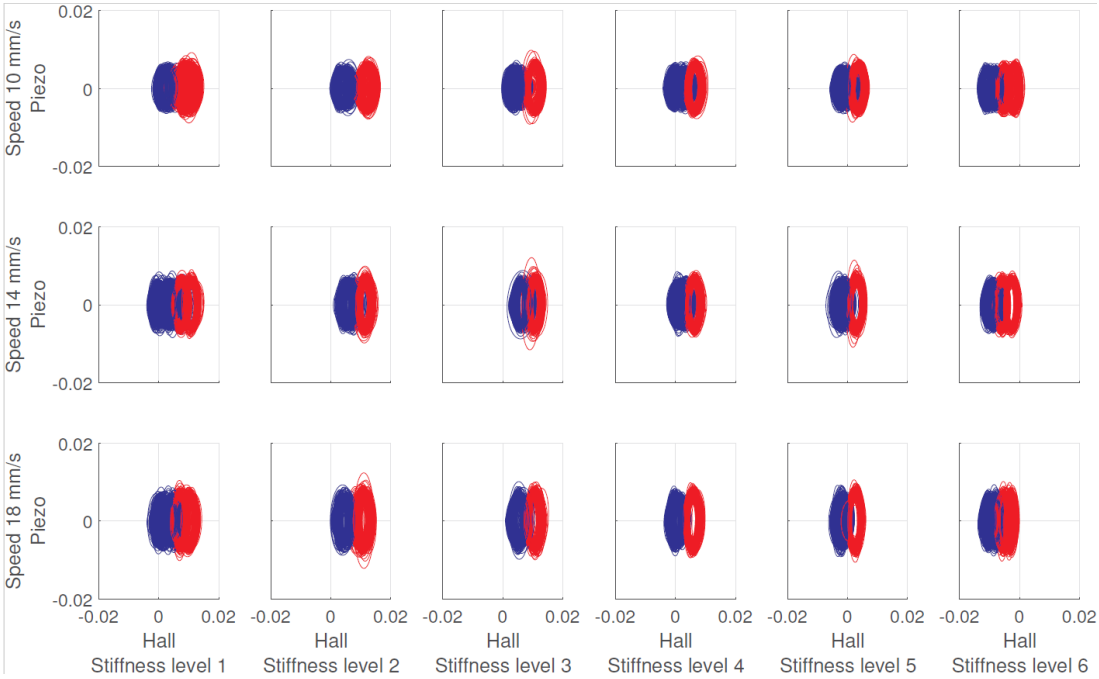

Figure 3.8: Covariance of Piezo and Hall sensor with stiffness and Speed for two materials. The red curves refer to the bins of the 3000 grit sandpaper, the blue curves refer to 5000 grit sandpaper.

These insights show that a robot using a rat whisker inspired VS-MWF can improve efficiency of classifying very similar textures by exploiting the interaction effect of whisking speed and the stiffness of the follicle that houses multiple modes of sensors. Furthermore, this sheds light on how and why rats may use stiffness control and whisking speed control for rapid object recognition in low visibility environments.

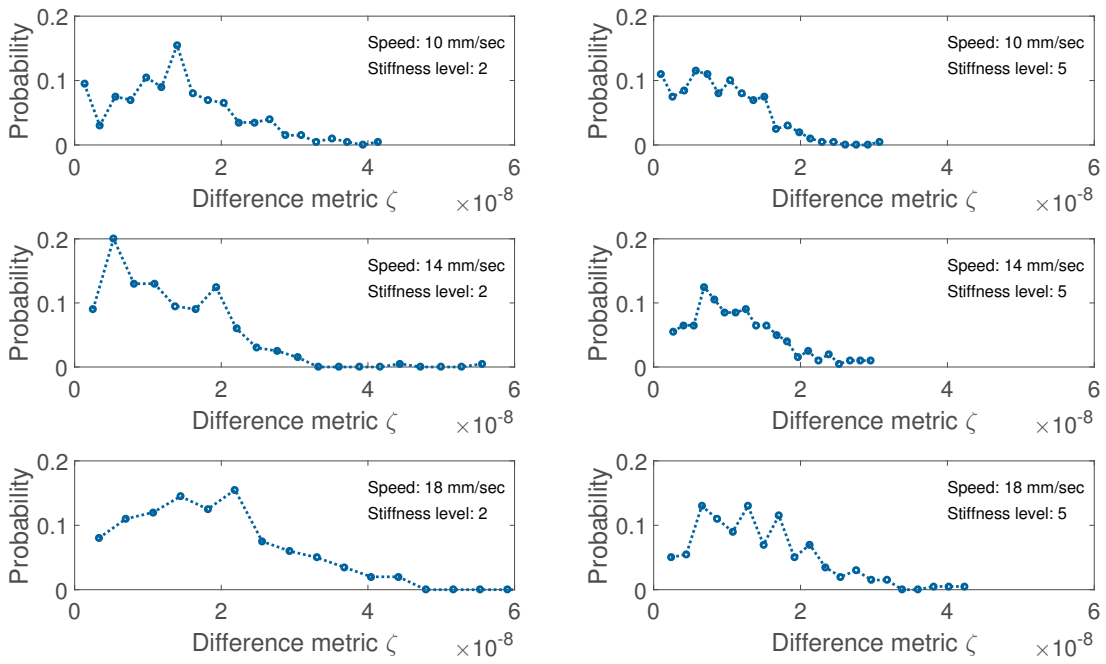

Figure 3.9: The probability distributions of Frobenius distance at a stiffness level and whisking speed. whisking speeds are 10mm/s for speed 1, 14mm/s speed 2 and 18mm/s speed 3. Stiffness levels are relative to the linear actuator displacement from 0 mm (stiffness level 1) to 10 mm (stiffness level 6) by 2 mm rises.

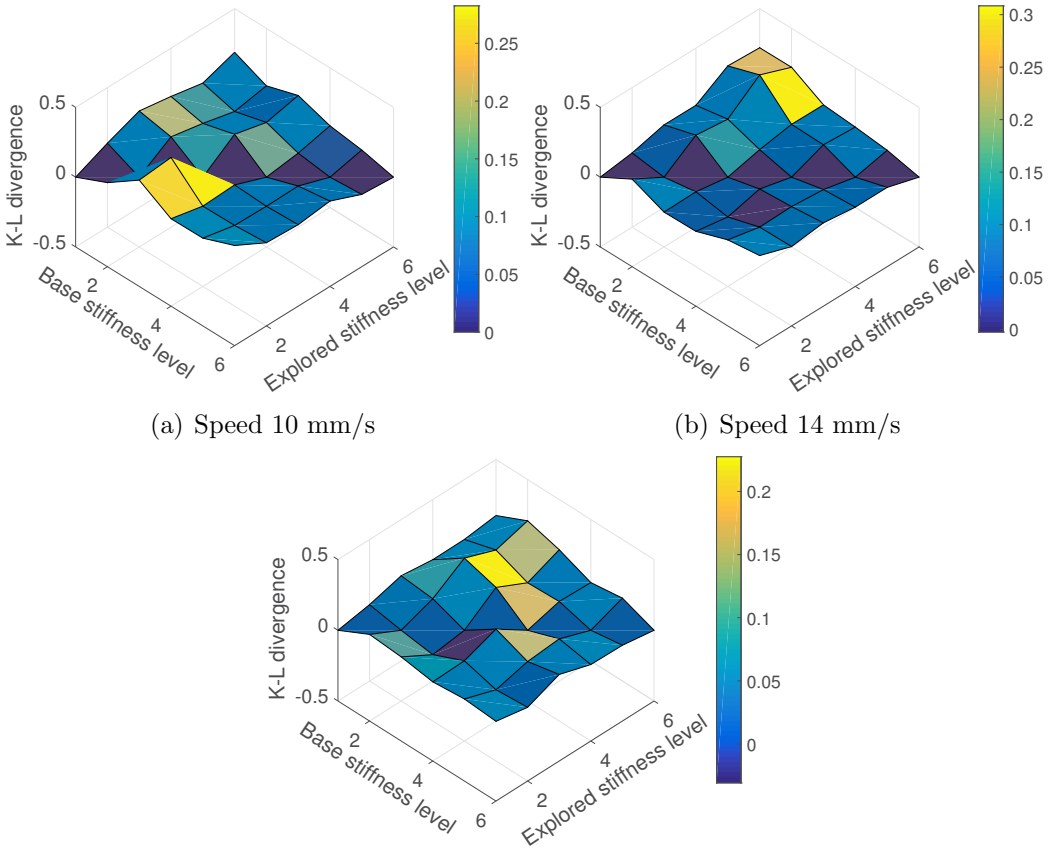

(a) Speed 10 mm/s

(b) Speed 14 mm/s

(c) Speed 18 mm/s

Figure 3.10: Information gain for the different speeds

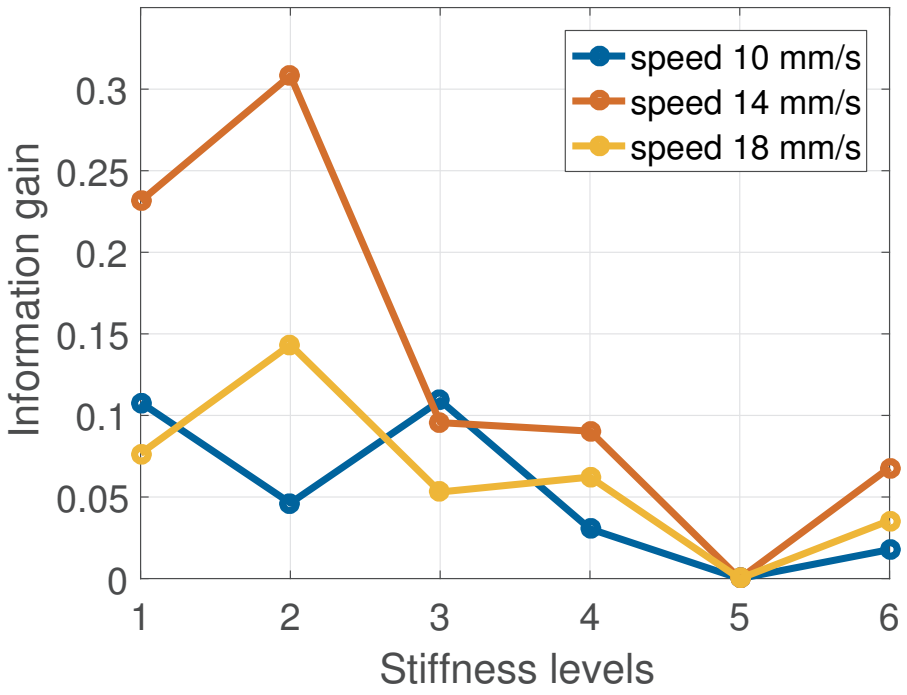

Figure 3.11: Information gain (K-L divergence) with stiffness levels and the whisking speed at the base stiffness 5. Whisking speeds are 10 mm/s, 14 mm/s and 18 mm/s. Stiffness levels are relative to the linear actuator displacement from 0 mm (stiffness level 1) to 10 mm (stiffness level 6) by 2 mm rises.

Chapter 4

Extended study of Stiffness Controllable Multimodal Whisker Follicle

---

In this chapter test the hypothesis that stiffness control in a multimodal robotic whisker follicle can capture more information in different regions of the frequency spectrum of whisker vibrations.

4.0.1 Stiffness Controllable Multimodal Whisker Sensor Characterization

The sensitivity of the sensors depends on the vibration of the whisker shaft and the stiffness of the silicone joint. When the whisker shaft vibrates, the shaft and silicone joint deform. These deformations generate vibrations on the Piezoelectric Sensor (PS) and the Permanent Magnet (PM) inside the WBS. The piezoelectric sensor's stress can be expressed by

$$\sigma_{\mathrm{PS}} = F_{\mathrm{PS}}/a_{\mathrm{PS}}, \tag{4.1}$$

where $F_{\mathrm{PS}} = k_{\mathrm{f}} w_{\mathrm{f}}$ is the lateral (shear) force exerting by the follicle on the piezoelectric disk, k_{f} is the variable stiffness of a spring in the simple model that simulates the disk lateral stiffness, w_{f} is this spring lateral deflection, and $a_{\mathrm{PS}} = 0.5[\mathrm{mm}^2]$ is the whisker-PS contacting area.

A cylindrical magnet is attached to the bottom end of the WSB. The magnet displacement generates a fluctuation in magnetic flux (B_{H}) around the Hall effect sensor. To calculate B_{H}, assume that the magnet and follicle axes are aligned, and the hall sensor is placed and (considering the small deformation of the beam) remains along the magnet axis despite the magnet displacement. Then from the formula for the magnetic flux on the the symmetry axis of an axially magnetised cylinder magnet [95] sensor have,

$$B_{\mathrm{H}} = \frac{B_{\mathrm{r}}}{2}\left(\frac{l_{\mathrm{PM}} + l_{\mathrm{MH}}}{\sqrt{r_{\mathrm{PM}}^2 + (l_{\mathrm{PM}} + l_{\mathrm{MH}})^2}} - \frac{l_{\mathrm{MH}}}{\sqrt{r_{\mathrm{PM}}^2 + l_{\mathrm{MH}}^2}}\right), \tag{4.2}$$

where $B_{\mathrm{r}} = 1.1\mathrm{T}$ is the residual magnetism of the cylindrical permanent magnet, $l_{\mathrm{PM}} = 2\mathrm{mm}$ and $r_{\mathrm{PM}} = 1\mathrm{mm}$ are the length and radius of the permanent magnet, respectively. l_{MH} is the PM-HS distance (see Fig. 4.1).

The variation of the electrical signals in PS and HS (Hall effect Sensor) can be related to the function of the superficial vibrissal nerve and the deep vibrissal nerve, respectively. The stiffness controllable silicone joint (k_{f}) mimics the ring sinus muscles in a biological whisker follicle. This controllable stiffness, as shown in section 4.1, influences the sensor signals by

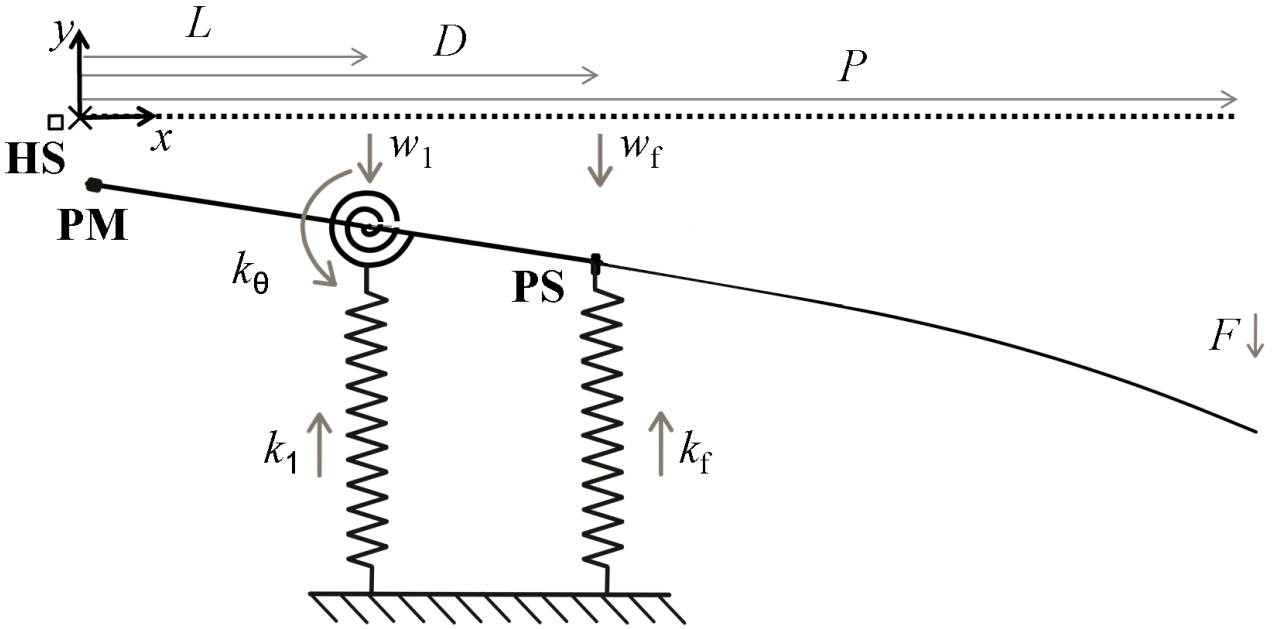

Figure 4.1: Schematic diagram of the whisker follicle with a Hall effect sensor (HS), a Permanent magnet (PM), and a piezoelectric sensor (PS). The soft joint is represented by a torsion (k_θ = 200N/rad) spring, a linear ($k_1 = 0.2$N/mm) spring at $x = L = 8$mm and a controllable stiffness spring (k_f) at $x = D = 13$mm. The applied force at the tip of the whisker is F. (x_0, y_0) is the model reference frame origin (shown with $(\times)$ in the figure)
, the whisker overall length is $P = 213$mm. w_1 and w_f denote the beam lateral displacement at the silicone joint and the piezoelectric sensor respectively.

changing the follicle vibration dynamics.

4.0.2 Whisker Modal Analysis

The whisker setup vibration dynamics is modeled as undamped modal analysis of a simple Euler-Bernoulli beam, with uniform cross-section and negligible axial strain and cross-section rotation compared to the beam shear strain. The relation between the external load and the whisker displacement and deformation can be expressed as follows [96]:

$$EI\partial^4 w/\partial x^4 + \rho a \partial^2 w/\partial t^2 = F(x,t), \tag{4.3}$$

where w is the beam lateral displacement, x is beam axial location, t is time, and $F(x,t)$ is the external load. $E = 228$GPa and $\rho = 1880$Kg/m^3 are the beam Elasticity modulus and density for the carbon fiber material, respectively. $a = \pi r^2$ $I = \pi r^4/4$, and $r = 0.25$mm are the beam

cross-section area, second moment of area, and radius, respectively.

Eq. 4.3 is a 4^{th}-order differential equation that presents the balance between the distributed loads, e.g. beam mass, along the beam. The balance of local shear loads, e.g. point masses and contacting springs, along the beam can be presented with a set of 3^{rd}-order differential equations. The effect of the attached springs to the beam that exert point loads at their contacting locations are captured as boundary conditions in these 3^{rd}-order differential equations. The boundary conditions related to the base linear ($k_1 = 0.2\text{N/mm}$) and torsion ($k_\theta = 200\text{Nm/rad}$) springs, and the stiffness variable linear spring (k_f) are given by load balance equations at the spring attachment points as [96, 97]:

$$\begin{aligned} EI\partial^3 w(L)/\partial x^3 + k_1 w(L) &= 0, \\ EI\partial^2 w(L)/\partial x^2 - k_\theta \partial w(L)/\partial x &= 0, \\ EI\partial^3 w(D)/\partial x^3 + k_\text{f} w(D) &= 0, \end{aligned} \tag{4.4}$$

The balance of moment is presented with a 2^{nd} order differential equation. The local shear force and moment are zero at the beam boundary conditions. Hence, the free ends boundary conditions can be derived as:

$$\partial^3 w(0|P)/\partial x^3 = \partial^2 w(0|P)/\partial x^2 = 0, \tag{4.5}$$

where $L = 8\text{mm}$, $D = 13\text{mm}$, and $P = 213\text{mm}$ are the position of the silicone joint, the piezoelectric sensor and the overall length of the beam, respectively. The time derivatives are not present here due to the lack of any point load along the beam (The sensors and magnet are considered to have zero masses). These boundary conditions are valid at any time.

To find the beam natural frequencies (ω_n) and mode shapes (W_{ω_n}), neglect $F(x,t)$ and follow the method of separation of variables by setting $w(x,t) = W(x)T(t)$, where $W(x)$ is a function that depends only on the spatial variable x and $G(t)$ is a function that depends only on the temporal variable t. By substituting the resulting system constant with $-\omega_n^2$, a Boundary Value

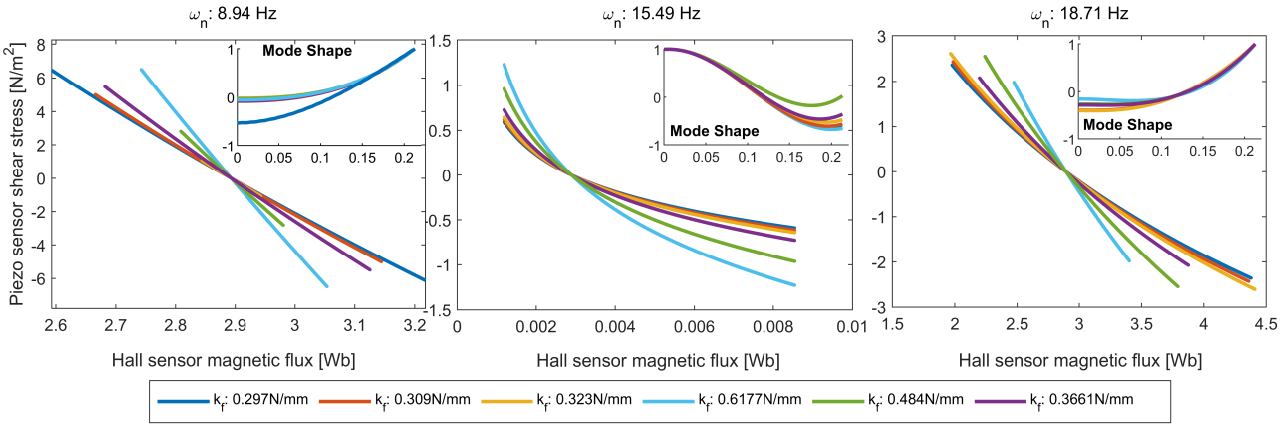

Figure 4.2: Simulated correlation between the induced piezoelectric sensor stress (σ_{PS}) and the Hall effect sensor flux (B_{H}) against the follicle stiffness for three different natural frequencies (ω_n) and $w_{\max} = 5$mm. Notice the different axes scales.

Problem (BVP) can be expressed for $W(x)$ as follows [96]:

$$EI\mathrm{d}^4W/\mathrm{d}x^4 - \rho a\omega^2 W = 0. \tag{4.6}$$

To be solved this BVP, the Matlab "bvp5c" function [97] have been used. The simulation parameters are chosen to closely match with experiment conditions.

The simulation results in Fig. 4.2 illustrates the mode shapes and correlation between the induced piezoelectric sensor stress (σ_{PS}) and the Hall effect sensor flux (B_{H}) against the follicle stiffness (found from experiments) for three different natural frequencies ($\omega_n \approx [8.9,\ 15.5,\ 18.7]$ Hz) and $w_{\max} = 1$mm. These results show that the correlation between the sensors reading may significantly change depending on the natural frequency of the system dominant mode of vibration. Also, the change of the follicle stiffness significantly affects the correlation between both sensors and the beam mode shape for the same natural frequency. This means that the follicle sensitivity can be changed by controlling the stiffness of the whisker follicle.

4.0.3 Experiment Setup

The experimental setup is shown in Fig. 4.3. The whisker sensor is attached horizontally to a 3D printed ABS plastic holder. This holder is connected to a 36cm L-shape rigid copper pipe

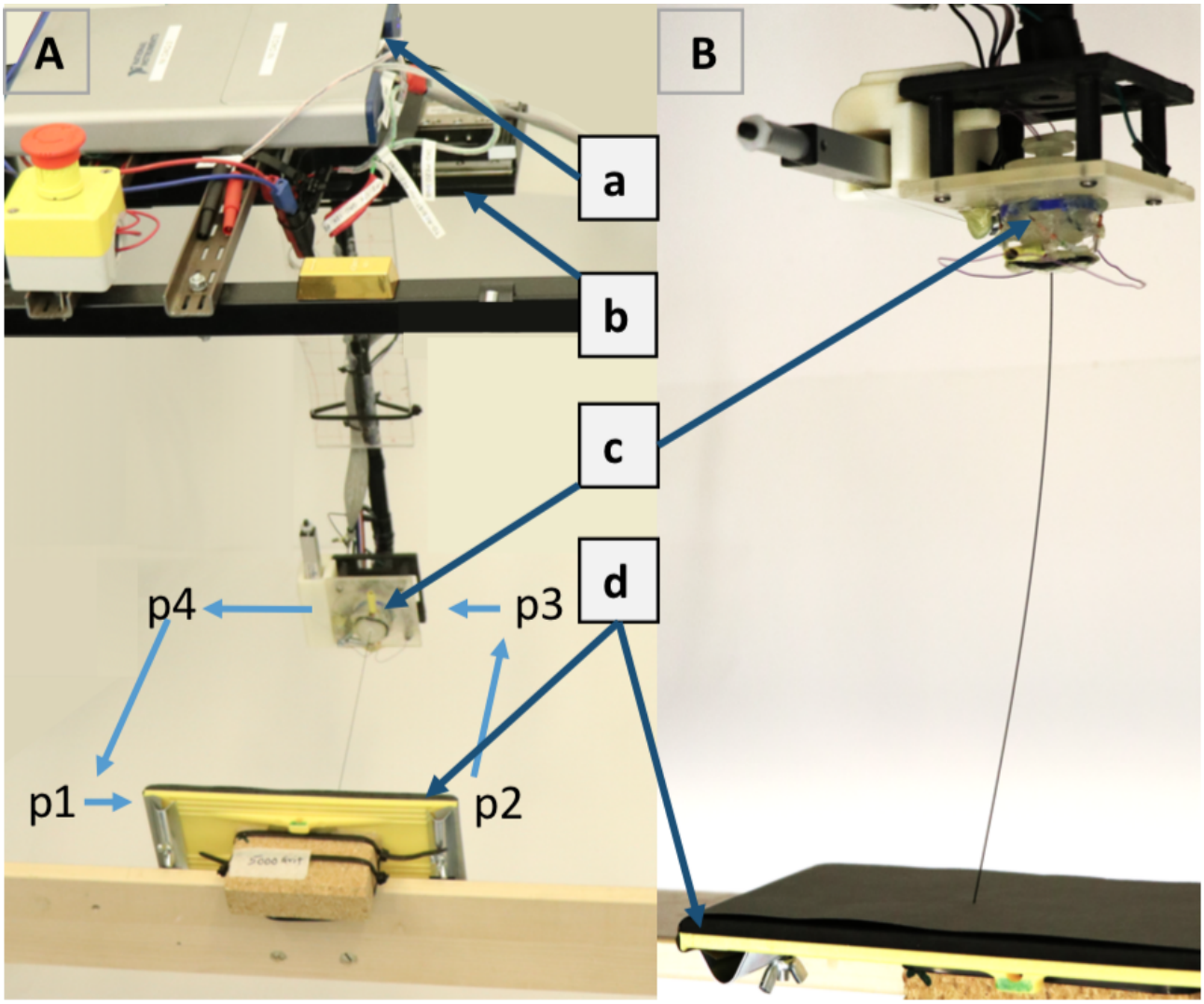

Figure 4.3: Experimental Setup (A) Hardware Setup and Programmed Path: (a) Data acquisition system (DAQ); (b) XY linear stage; (c) variable stiffness multimodal whisker follicle (VS-MWF); (d) Sandpaper holder; Programmed Path is $p1$, $p2$, $p3$ and $p4$ (Data is recorded only when the Whisker shaft moves from $p1$ to $p2$). (B) VS-MWF probing against a sandpaper.

arm whose longest side is strengthened using an acrylic sheet. The end corresponding to the longest side of this arm is attached to the XY stage (Aerotech- ANT130-160-XY) through a 70×70×5mm rigid 3D printed ABS plastic plate. This stage allows controlling the movement of the whisker sensor along the **x** and **y** coordinates.

A National Instrument NI DAQ USB-6341 Multifunction I/O Device together with a LabView2016 interface was used to acquire signals from the whisker sensor at a 10kHz sampling rate and to control the RRM, and XY linear stage. MatLab R2016a, Mathworks Inc, was employed for the post-processing and analysis of the data.

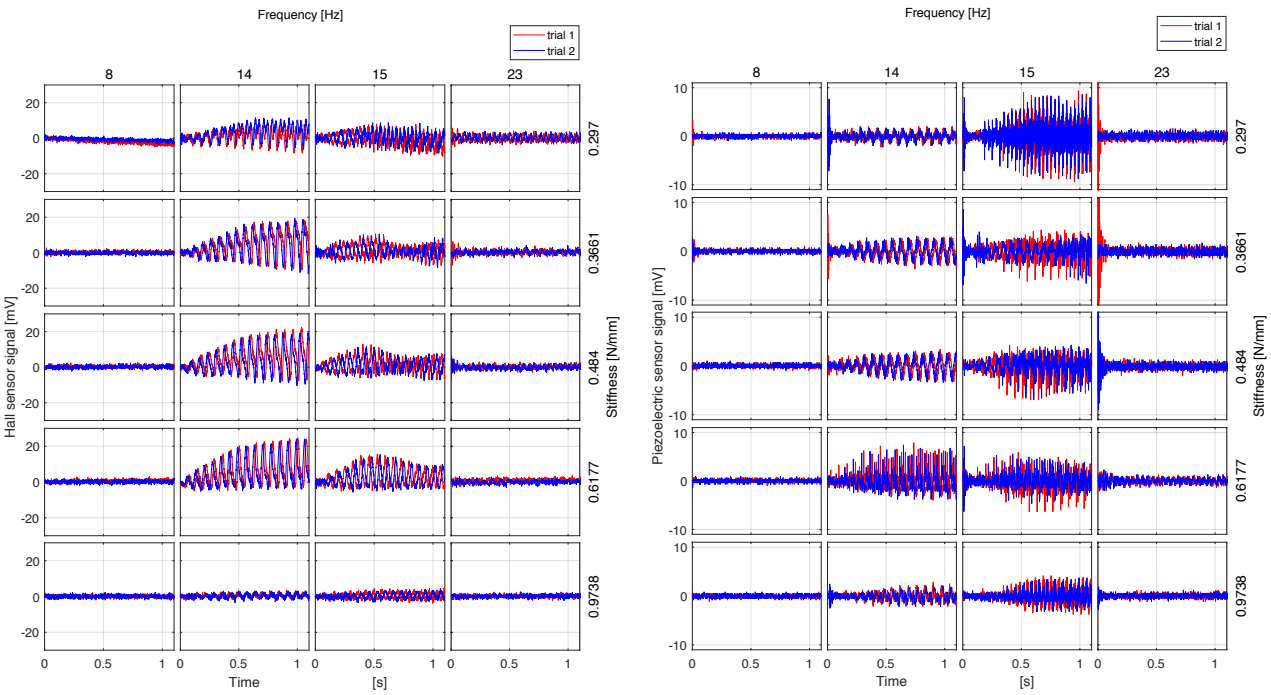

Figure 4.4: (a) Raw data of Hall effect sensor for different frequencies and stiffness, (b) Raw data of piezoelectric sensor for different frequencies and stiffness

Experiment-1: Characterisation of the natural frequency of the VS-MWF

In this initial experiment, the whisker follicle was vibrated for 30 cycles from 8Hz to 23Hz in 1Hz steps (16 frequency steps in total) to understand the frequency response of the free whisker and follicle (whisker not touching a surface). The magnitude of oscillation along the y-axis of the stage has been chosen arbitrarily at 0.5mm.

In this experiment use stiffnesses 0.2970, 0.3090, 0.3230, 0.3661 ,0.4840, 0.6177, 0.8328, 0.9622 and 0.9738N/mm (Stiffness obtain by using the ATI nano17 Force Sensor) for each frequency. Initially, the stiffness is set to 0.2970N/mm (carbon shafts inserted at the lowest level into the silicone tubes attached to the WSB joint), which provides a default stiffness of the silicone joint. The corresponding initial frequency of the whisker sensor is set to 8Hz. In a set of trials, the whisker vibrates 30 cycles, then stops and stabilizes at its initial position. For each combination of stiffness levels and frequency levels, acquired data for 2 trials of 30 cycles each.

Extract the first 100 samples (10ms) in each trial to compute the base level readings of both the Hall and piezoelectric sensors and subtracted this from the raw data to obtain signals that

are caused due to the oscillations.

Experiment-2: The behavior of the VS-MWF in texture discrimination

In the second experiment, the whisker was programmed to probe along the rough side of 12 sandpaper samples (80, 240, 320, 400, 600, 800, 1000, 1200, 2000, 3000, 5000, 7000 grit roughness) for a 7.5cm span as shown in Fig. 3.2. The whisker was moved to the edge of a sandpaper holder with an indention of 3mm before starting to sweep across the sandpaper at different speeds. I chose a 3mm indentation based on previous results from the chapter two.

In the experiment, one sandpaper sample is fixed to the external holder and clamped perpendicular to the whisker shaft (Fig. 3.2). Initialization of the experiment for each sandpaper sample is identical for all the iterations. By following the path shown in Fig. 3.2.A, the whisker sensor comes into contact with the surface of the sandpaper. These movements are controlled through the usage of the XY stage. The stiffness of the whisker follicle use the following values 0.2970, 0.3090, 0.3230, 0.3661, 0.4840, 0.6177, 0.8328, 0.9622 and 0.9738 N/mm similar to the 4.0.3. In this experiment use 3mm contact indentation across all iterations and 10mm/s, 14mm/s, 18mm/s, whisking speeds. Initially, the stiffness is set to 0.2970N/mm, as the default stiffness of the silicone joint between the two sensors of the whisker follicle and the corresponding whisking speed of the whisker sensor is set to 10mm/s. For each combination of stiffness levels and contact speed, acquired data for 2 trials. Therefore, for a given stiffness, the three contact speeds gave 6data sets for a single sandpaper.

4.0.4 Calculation of distance between distribution of textures

Extract base subtracted data as described in the last paragraph of section 4.0.3. The Hall and piezoelectric sensor data were divided into 200 bins to construct a distribution of root mean square (RMS) values to compare two textures. A distance metric between these distributions for two textures was computed to understand how the follicle stiffness and whisking speed influences the distance metric.

Quantify distance between RMS distributions of textures A and B, using the standardized Euclidean Distance (SED) given by

$$SED_{AB} = \sqrt{\frac{\Sigma(\mathbf{RMS_A} - \mathbf{RMS_B})^2}{\sigma_A \sigma_B}} \tag{4.7}$$

where, $\mathbf{RMS_A}$ is a vector of RMS values of sensor readings in 200 time bins when the whisker is brushed on one material (12 sandpapers from 80 - 7000 grit) and $\mathbf{RMS_B}$ is that for the reference sample (80 grit sandpaper). The corresponding standard deviations are σ_A and σ_B. In this case, SED_{AB} is the standardized Euclidean Distance between the RMS values of sensor data across 200 bins in a given brushing trial corresponding to two sandpapers. The normalized SED used, hereafter referred as $NSED$ for clarity of comparison.

4.1 RESULTS

4.1.1 Numerical simulation results

Fig. 4.2 shows numerical simulation results based on the model derived in section 4.0.2. The analytical model predicts that the stiffness can be used to rotate the covariance between the Hall effect sensor and the piezoelectric sensor for a given whisker vibration. In other words, the stiffness of the follicle is a useful internal parameter to bias perception in the frequency domain.

4.1.2 Signal amplitude variation with follicle stiffness and free oscillation frequency

Fig. 4.4 (a) and (b) show the base subtracted raw experimental readings (see section 4.0.3 in the methods section for details) from the Hall effect sensor and the piezoelectric sensor mounted in the VS-MWF for selected levels of oscillation frequencies (8, 14, 15 and 23 Hz) and stiffnesses 0.2970, 0.3661, 0.4840, 0.6177 and 0.9738 N/mm. This can observe a higher magnitude in

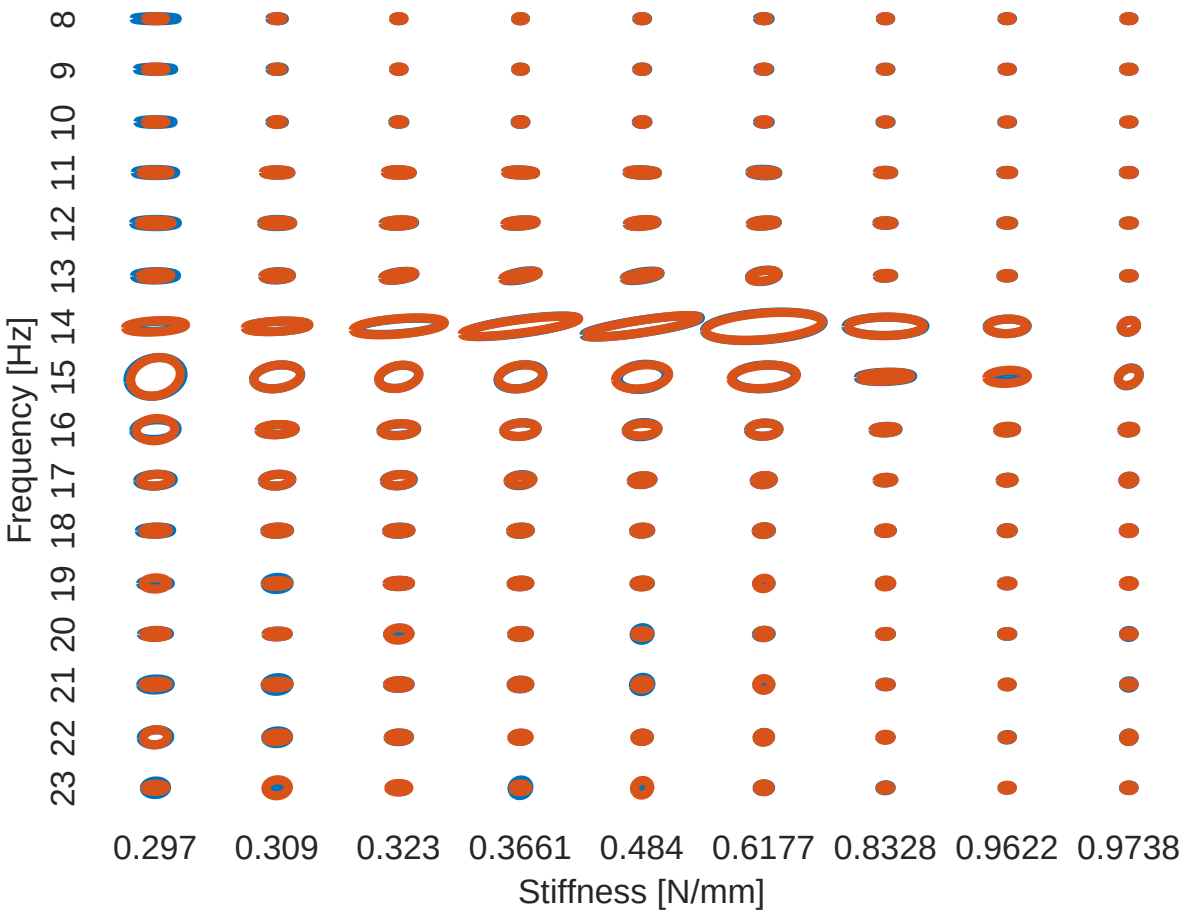

Figure 4.5: Covariance of Piezoelectric and Hall effect sensor signals for different combinations of stiffness and frequency for free whisker (whisker not touching a surface) and follicle vibrations . Red and blue ellipses refer to trials 1 and 2, respectively. Axes ranges are not shown for clarity. x and y axes are normalized to respect the aspect ratio. The range of the axes are from -0.0210 to 0.0210 and from -0.0069 to 0.0069 respectively for x and y. The shape of the ellipsoids represents the Eigenvalues of the principal components of each covariance matrix.

the signals for 14-15Hz oscillation frequency. Also I can see that the magnitude variation is depending on the stiffness of the VS-MWF.

Fig. 4.5 shows the covariance ellipses between the two sensor modalities for different combinations of follicle stiffness and oscillation frequencies. The variation of the size of the ellipses shows that follicle stiffness helps to rotate the Eigenvectors of the covariance matrix and that the maximum Eigenvalues correspond to oscillation frequencies between 12 - 16Hz.

These results provide important clues to acquire information in the frequency domain for texture classification by maximizing the signal to noise ratio of measurements. To demonstrate this

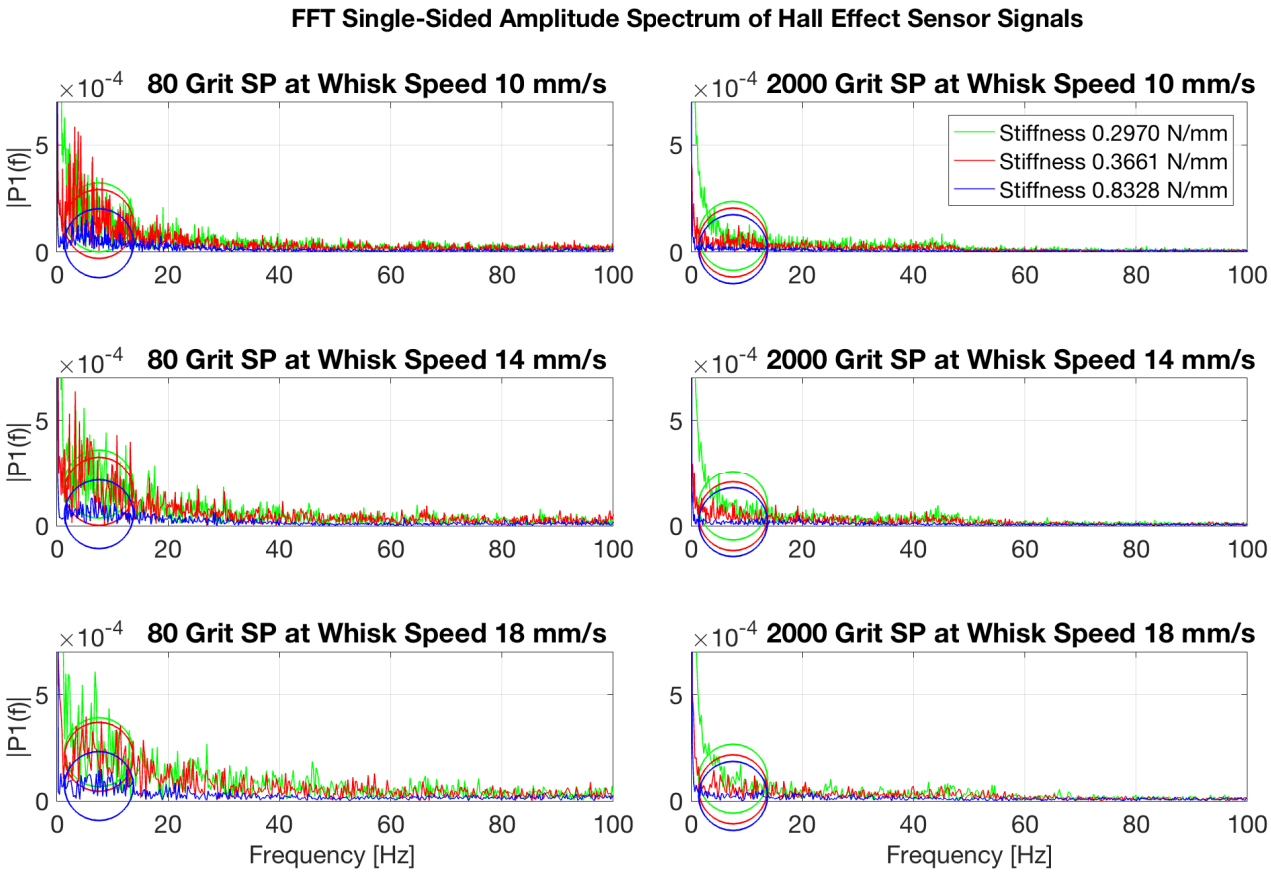

Figure 4.6: FFT of Hall effect sensor data at follicle stiffness 0.2970N/mm, 0.3661N/mm, 0.8328N/mm and whisking speed 10mm/sec, 14mm/sec ,18mm/sec on 80, 2000 grit sandpapers.

effect, I did a second experiment that involves distinguishing 12 pairs of sandpapers (80 - 7000 grit) described in more detail in section 4.0.3.

4.1.3 Maximizing a difference metric for texture classification

Fig. 4.6 and Fig. 4.7 show the fast Fourier transform (FFT) single-sided amplitude spectrum of the Hall effect sensor and Piezoelectric sensor signals at 0.2970N/mm, 0.3661N/mm, 0.8328N/mm follicle stiffness and whisking speeds 10mm/sec, 14mm/sec ,18mm/sec on 80, 2000 grit sandpapers. Here I can notice that the hall effect sensor produces high power amplitude in the low-frequency region ($0 - 40$ Hz) and Piezoelectric sensor produces high power amplitude in the high-frequency region (100 Hz and above). The circles show the median value of the particular distribution at above described follicle stiffness values. The circles show the hall effect sensor produces high power low frequency components at low stiffness values. Moreover,

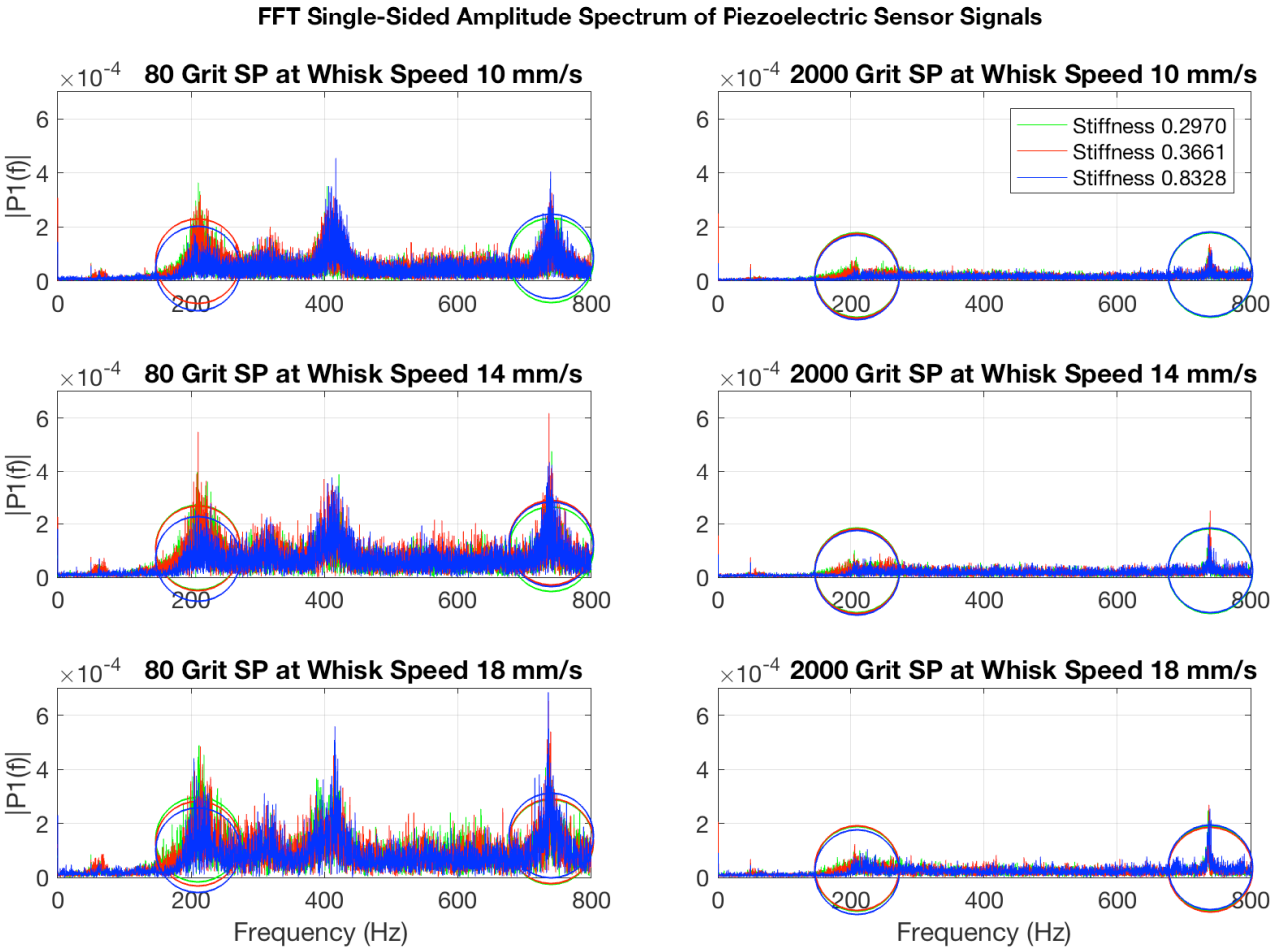

Figure 4.7: FFT of Piezoelectric sensor data at follicle stiffness 0.2970N/mm, 0.3661N/mm, 0.8328N/mm and whisking speed 10mm/sec, 14mm/sec, 18mm/sec on 80, 2000 grit sandpapers.

the hall effect sensor FFT shows a frequency shift with the change of stiffness. The circles on Fig. 4.7 shows that the piezoelectric sensor produces low power low frequency components and high power high frequency components. This effect increases with increasing follicle stiffness. Interestingly, with low stiffness, it produces high power amplitude on low frequencies and low power amplitude on high frequencies. Therefore, the piezoelectric sensor with variable stiffness contributes to filter signals. This phenomenon implies that the interaction effect of the speed of whisking with follicle stiffness help to capture information in different frequency components in the frequency domain and for the texture classification task.

Fig. 4.8 shows the NSED of RMS values of the Hall-effect sensor and the Piezoelectric sensor data of 12 different grit level of sandpapers at nine stiffnesses 0.2970, 0.3090, 0.3230, 0.3661, 0.4840, 0.6177,0.8328, 0.9622, 0.9738 N/mm and three whisking speeds of 10, 14, 18 mm/s.

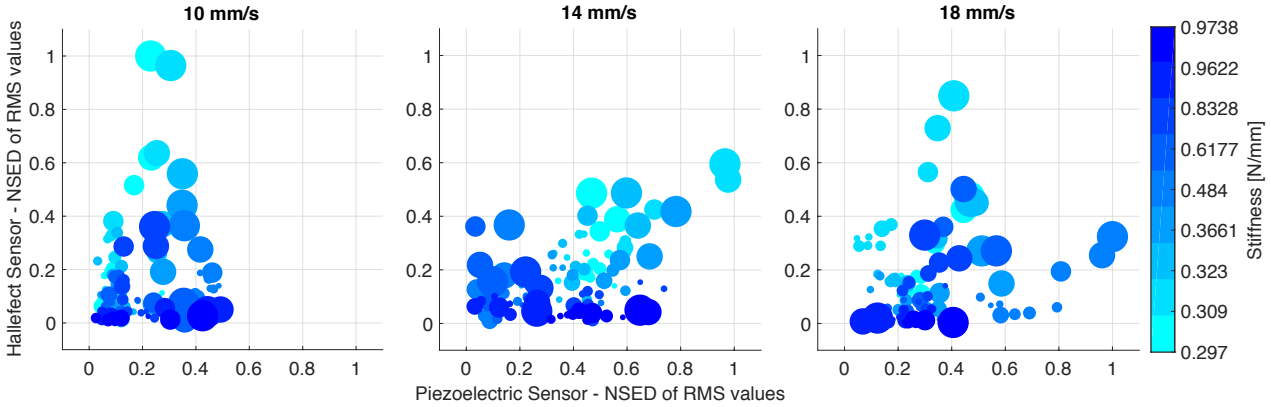

Figure 4.8: NSED - Normalize Standardized Euclidean Distance of RMS values computed using equation (4.7). The smallest circle represent the rough sandpaper, and the largest circle represent the smoothest sandpaper. At a given speed, the Standardized Euclidean Distance of the RMS values used to compare between roughest sandpaper (80 grit) against all other sandpapers. The sandpaper grit values are 80, 240, 320, 400, 600, 800, 1000, 1200, 2000, 3000, 5000, 7000.

The largest circles represent the smoothest (7000 grit) sandpaper, and the smallest represent the rough (240 grit) sandpaper. The RMS values of the two sensor modalities corresponding to the 80 grit sandpaper were used as the reference to compute the NSED for all other sandpapers.

The study shows that the sensor at the low whisking speed at low stiffness favor the hall effect sensor by producing a higher NSED. Moreover, when the whisking speed and stiffness increases, NSED of piezoelectric sensor increases disproportionately compared to the Hall effect sensor. Essentially the follicle stiffness allows the sensor to bias itself in the frequency domain for the given speed of whisking.

This observation also shows that the Hall effect sensor captures the low-frequency region (i.e. the geometric features of an object) and the piezoelectric sensor captures the high-frequency region (i.e. the texture of objects) . **The substantial benefit of using the multi-modal follicle is therefore being able to capture different vibration frequencies by controlling the stiffness of the follicle together with the whisking speed. This is very useful for a robot to acquire texture and geometry information of an object in real time.**

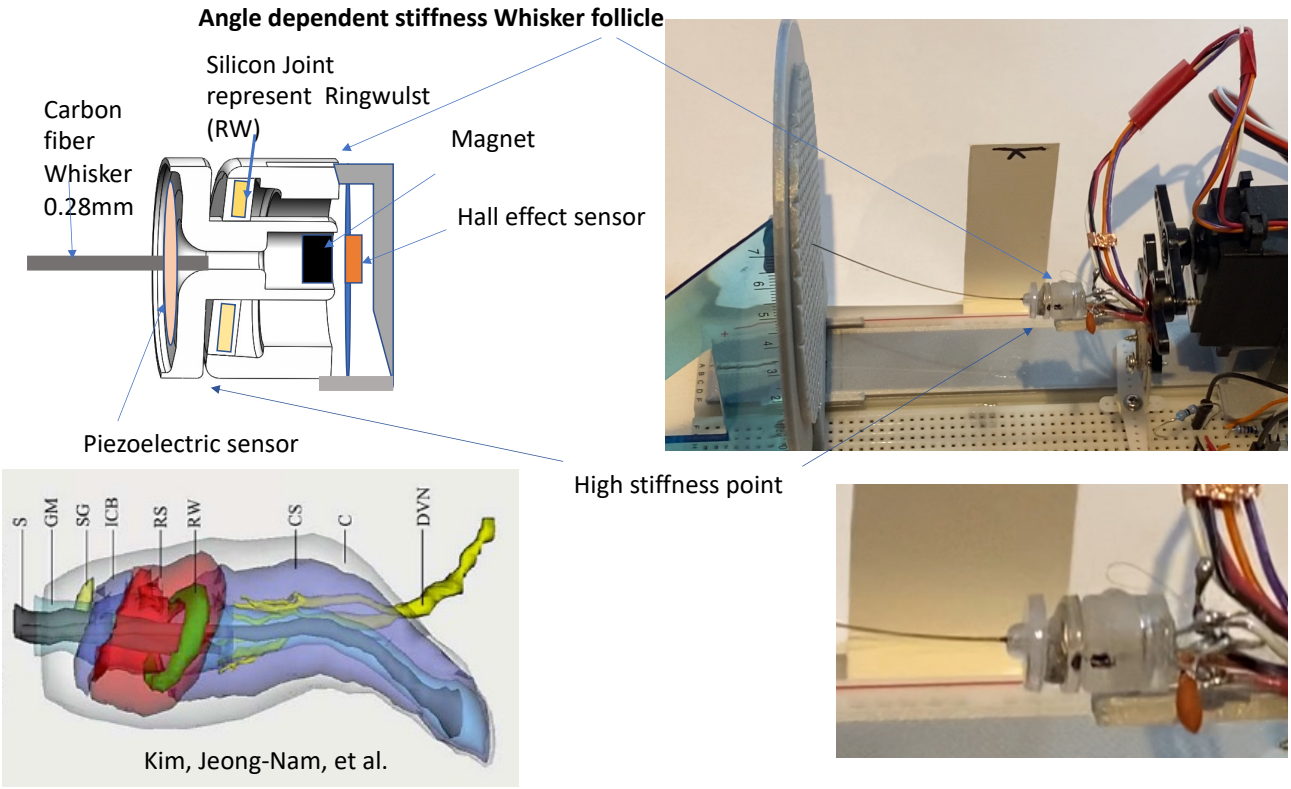

Figure 4.9: Angle dependent stiffness in the whisker follicle inspired by Ringwulst(RW). This is actuated by servo motor and it change the stiffness while rotating

4.1.4 Angle Dependent Stiffness in the Whisker Follicle Helps to Arbitrate Multimodal Vibrisal Perception

These Fig. 4.11 Fig. 4.10 show the continuous wavelet transform (CWT) of piezoelectric and hall effect sensor data. it shows with change of stiffness causes frequency shift. These insights show that a robot using a rat whisker inspired VS-MWF can improve the efficiency of identifying objects by exploiting the interaction effect of whisking speed and the stiffness of the follicle that houses multiple modes of sensors with a multi-modal whisker follicle.

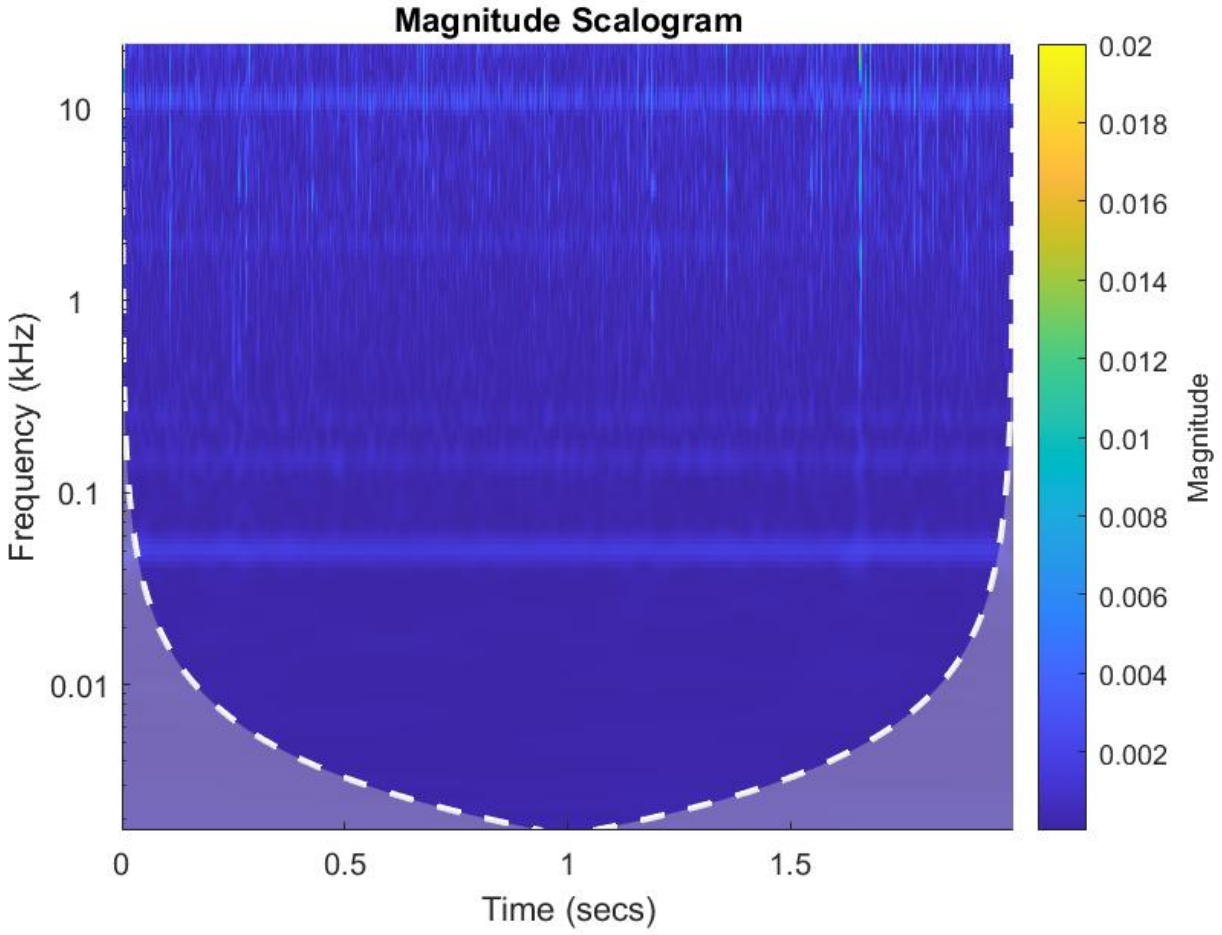

Figure 4.10: Continuous wavelet transform on Hall-effect sensor raw data. Highest stiffness in between 0.5s to 1.5s.

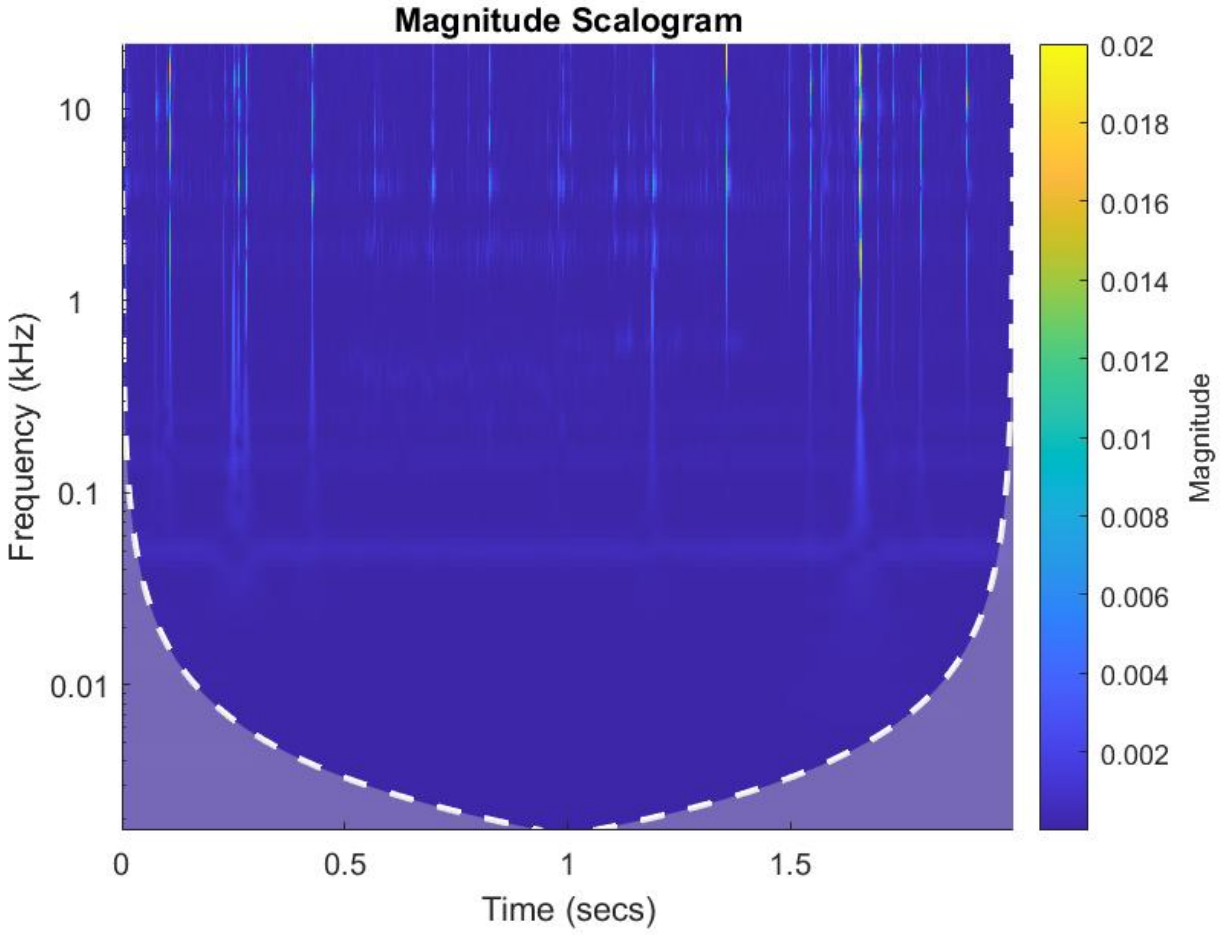

Figure 4.11: Continuous wavelet transform on piezoelectric sensor raw data. Highest stiffness in between 0.5s to 1.5s .

Chapter 5

Conclusion

5.1 Summary of the Research Achievements

This research details a novel whisker sensor system, that incorporates two different sensors, used in order to transduce information regarding textures of a sample object. The Hall-effect sensor and piezoelectric sensor provide frequency-dependent data relative to vibrations on a carbon-fiber whisker shaft. The whole system is movable and therefore it is capable of producing 'whisking' movements. The design was tested for different levels of contact speed and indentation.

The maximum eigenvalue of the covariance matrix for the two sensors in the follicle - piezoelectric and Hall sensor - represents the overall sensitivity of the whisker system. The angle of the eigenvector corresponding to the maximum eigenvalue gives the relative contribution made by the two sensors in the follicle.

From the analysis of the results in chapter two, it can be concluded that that increasing indentation causes the maximum eigenvalue to increase, before it settles at a stable value. The angle of the eigenvector corresponding to the highest eigenvalue and its variability is sensitive to the speed of whisking at lower indentation levels. They settle down at a steady range beyond an indentation of 3mm.

These results indicate that the information gain of low and high frequency features of the object can be controlled by selectively controlling the whisking speed and indentation within an optimum range. This not only provides new insights to design multi-modal robotic whisker follicles but also sheds light on our understanding about the functionality of mammalian whisker follicles.

The experimental result presented in this research agrees with previous claims and methods shown in previous studies. For instance, Pearson et al. described a whisking pattern with the aim of *'minimal impingement/maximal contact (MIMC)'* [47]. I predict that a similar method would be effective for the design, as data from indentations is best below a certain threshold (3 mm), and information at higher contact speeds gives better sensitivity. The benefits of lower levels of indentation mean sensors with a smaller dynamic range but a larger sensitivity could be employed, whilst there is also less risk of damage to the system, if the forces on the whiskers are reduced. Applying this concept, whisker can actively choose its' behavior during such a whisking activity given different environments to maximise the information gained, for instance, in modality of texture classification similar to the previous study [45], [50]. Several works, such as those mentioned previously, employ designs of tactile sensor systems with multi-modal sensors. These include designs inspired from the human fingertip, [98], [99], contact sensing and active whisker sensors, [47], [50], and designs inspired by insect antennae, [42], [100]. However, most of work in this research field has not specifically addressed the low dimensional information such as the principle components of co-variation in high and low frequency sensory modalities. Although whisking methods have been implemented in several works, little has been done to test and find optimal whisking speeds and indentations for movable whiskers.

This research for the first time provides significant insights into how the whisking behavior is related to the correlation of multiple sensory information presented by the eigeninformation of the covariation of data, which can be used under information gain metrics [93] to identify the texture of an object.

Furthermore, there is no clear explanation on what the ring muscle structure between the superficial and deep vibrassal nerves does in terms of tactile information

gain [101] [27] [102]. In this research tested the hypothesis that a similar mechanism to control the stiffness of the follicle may lead to mutual information gain in a multi-modal sensing in a controllable stiffness whisker follicle.

The study in chapter three used a robotic approach to test the above hypothesis using a novel variable stiffness multi-modal whisker sensor (VS-MWS) system, that transduce information on textures of sample objects. The whisker sensor contains a stiffness controllable joint in-between the hall sensor and the piezoelectric sensor which provides frequency-dependent data corresponding to vibrations on a carbon-fibre whisker shaft. The system is capable of generating vibration itself or producing 'whisking' movements as it is attached to a movable platform. Initially, the design was tested for frequency response in different stiffness configurations. Then, the VS-MWS was tested for different levels of stiffness and contact speeds to test its ability to distinguish two similarly lookalike objects.

The experimental results show that the sharpness of the probability distribution of the Frobenius distance between the covariance matrices corresponding to the two textures can be increased as a combined effect of follicle stiffness and whisking speed. This implies that follicle stiffness plays an important role in information gain in texture classification tasks.

The study in chapter four tested a novel variable stiffness multimodal whisker sensor (VS-MWS) for its ability to distinguish pairs of sandpapers for different follicle stiffnesses and whisking speeds. The sandpapers used because their smoothness can be quantified using the grit number. **The experimental results show for the first time that a multimodal sensor can help to move the bandwidth of signal gain from low to high frequency information of textures by changing the stiffness and whisking speed.**

These findings provide important design guidelines for future robots using whiskers to help them navigate in uncalibrated environments. In particular, these findings show **that the efficacy of robotic whiskers can be improved by using multi-modal transduction embedded in a controllable stiffness follicle, whereby the vibration dynamics of the follicle can be used to induce mutual information that the sensors cannot acquire in isolation.**

In addition to implications in robotics, these findings also make predictions about the rat whisker follicles. Authors in [101] have found that the morphology and mechanics provide the basis for a pre-neural computation of rat vibrissal information (afferent signals). However, the contribution of the ring muscle structure between the superficial and deep vibrissal nerves of the rat whisker follicle in terms of capture information has not been fully understood so far [101] [27] [103]. The findings in this study predict that this mechanism to control the stiffness of the follicle may lead to capturing information across a broad frequency spectrum using a controllable stiffness whisker follicle.

Moreover, this study sheds light on how and why rats may use stiffness control and whisking speed control for quick object recognition in low visibility environments for their survival.

There are several previous studies that consider the role of whisker shaft stiffness and the probing pattern in tactile sensing. For instance, authors in [104] observed that a stiffer whisker would increase the sensitivity of a piezoelectric transducer attached to the whisker. Pearson et. al., described a biomimetic whisking pattern [47], and Sornkarn [105] found that internal stiffness of a probe can help to gain information during soft tissue palpation. These findings consolidate those in [105] in a multimodal sensing context.

Studies into biological rat whisker follicle agree with the results. For instance, authors in [101] have found that the morphology and mechanics provide the basis for a preneural computation of rat vibrissal information (afferent signals).

Furthermore, this research shows the usefulness of robotic approaches to understand intractable biological phenomena, such as the design in this research employs two different sensors, stiffness control, and reflects the fact that in nature, several different transduction techniques, and several different types of nerve endings are used to obtain tactile information about the environment. The method and design in this research show that biomimicry is a good way to provide new sensors and techniques in robotics.

In conclusion, this study for the first time delivers substantial insights into how the stiffness control in a whisker follicle is associated with multiple sensory information capture in texture

classification.

Figure 5.1: Scan QR code to watch experiment videos.

Bibliography

[1] T. J. Park, C. Comer, A. Carol, Y. Lu, H.-S. Hong, and F. L. Rice, "Somatosensory organization and behavior in naked mole-rats: Ii. peripheral structures, innervation, and selective lack of neuropeptides associated with thermoregulation and pain," *Journal of comparative neurology*, vol. 465, no. 1, pp. 104–120, 2003.

[2] R. A. Grant, B. Mitchinson, C. W. Fox, and T. J. Prescott, "Active touch sensing in the rat: anticipatory and regulatory control of whisker movements during surface exploration," *Journal of neurophysiology*, vol. 101, no. 2, pp. 862–874, 2009.

[3] A. S. Ahl, "The role of vibrissae in behavior - a status review." *Veterinary Research Communications*, vol. 10, no. 4, pp. 245–268, 1986.

[4] M. E. Diamond, M. Von Heimendahl, P. M. Knutsen, D. Kleinfeld, and E. Ahissar, "'where'and'what'in the whisker sensorimotor system," *Nature Reviews Neuroscience*, vol. 9, no. 8, pp. 601–612, 2008.

[5] T. J. Prescott, M. E. Diamond, and A. M. Wing, "Active touch sensing," 2011.

[6] G. Dehnhardt, B. Mauck, and H. Bleckmann, "Seal whiskers detect water movements," *Nature*, vol. 394, no. 6690, pp. 235–236, 1998.

[7] O. Fitzgerald, "Discharges from the sensory organs of the cat's vibrissae and the modification in their activity by ions," *The Journal of physiology*, vol. 98, no. 2, pp. 163–178, 1940.

[8] R. Stephens, I. Beebe, and T. Poulter, "Innervation of the vibrissae of the california sea lion, zalophus californianus," *The Anatomical Record*, vol. 176, no. 4, pp. 421–441, 1973.

[9] R. A. Grant, V. Breakell, and T. J. Prescott, "Whisker touch sensing guides locomotion in small, quadrupedal mammals," *Proceedings of the Royal Society B*, vol. 285, no. 1880, p. 20180592, 2018.

[10] R. W. Dykes, "Afferent fibers from mystacial vibrissae of cats and seals," *Journal of Neurophysiology*, vol. 38, no. 3, pp. 650–662, 1975.

[11] R. W. Berg and D. Kleinfeld, "Rhythmic whisking by rat: retraction as well as protraction of the vibrissae is under active muscular control," *Journal of neurophysiology*, vol. 89, no. 1, pp. 104–117, 2003.

[12] D. N. Hill, R. Bermejo, H. P. Zeigler, and D. Kleinfeld, "Biomechanics of the vibrissa motor plant in rat: rhythmic whisking consists of triphasic neuromuscular activity," *Journal of Neuroscience*, vol. 28, no. 13, pp. 3438–3455, 2008.

[13] M. Brecht, B. Preilowski, and M. M. Merzenich, "Functional architecture of the mystacial vibrissae," *Behavioural brain research*, vol. 84, no. 1-2, pp. 81–97, 1997.

[14] G. E. Carvell and D. J. Simons, "Biometric analyses of vibrissal tactile discrimination in the rat," *Journal of Neuroscience*, vol. 10, no. 8, pp. 2638–2648, 1990.

[15] E. Guić-Robles, C. Valdivieso, and G. Guajardo, "Rats can learn a roughness discrimination using only their vibrissal system," *Behavioural brain research*, vol. 31, no. 3, pp. 285–289, 1989.

[16] T. Prigg, D. Goldreich, G. E. Carvell, and D. J. Simons, "Texture discrimination and unit recordings in the rat whisker/barrel system," *Physiology & behavior*, vol. 77, no. 4-5, pp. 671–675, 2002.

[17] M. Von Heimendahl, P. M. Itskov, E. Arabzadeh, and M. E. Diamond, "Neuronal activity in rat barrel cortex underlying texture discrimination," *PLoS Biol*, vol. 5, no. 11, p. e305, 2007.

[18] B. Mitchinson, C. J. Martin, R. A. Grant, and T. J. Prescott, "Feedback control in active sensing: rat exploratory whisking is modulated by environmental contact," *Proceedings of the Royal Society B: Biological Sciences*, vol. 274, no. 1613, pp. 1035–1041, 2007.

[19] M. J. Hartmann, "Active sensing capabilities of the rat whisker system," *Autonomous Robots*, vol. 11, no. 3, pp. 249–254, 2001.

[20] L. Estebanez, J. Bertherat, D. E. Shulz, L. Bourdieu, and J.-F. Léger, "A radial map of multi-whisker correlation selectivity in the rat barrel cortex," *Nature communications*, vol. 7, no. 1, pp. 1–8, 2016.

[21] N. C. Roy, T. Bessaih, and D. Contreras, "Comprehensive mapping of whisker-evoked responses reveals broad, sharply tuned thalamocortical input to layer 4 of barrel cortex," *Journal of neurophysiology*, vol. 105, no. 5, pp. 2421–2437, 2011.

[22] E. Lottem and R. Azouz, "Mechanisms of tactile information transmission through whisker vibrations," *Journal of Neuroscience*, vol. 29, no. 37, pp. 11 686–11 697, 2009.

[23] M. Brecht, B. Preilowski, and M. Merzenich, "Functional architecture of the mystacial vibrissae." *Behavioural Brain Research*, vol. 84, no. 1–2, pp. 81–97, 1987.

[24] L. Bosman, A. Houweling, C. B. Owens, N. Tanke *et al.*, "Anatomical pathways involved in generating and sensing rhythmic whisker movements." *Frontiers in Integrative Neuroscience*, vol. 5, 2011.

[25] G. Carvell and D. Simons, "Biometric analyses of vibrissal tactile discrimination in the rat." *Neuroscience*, vol. 10, no. 8, 1990.

[26] S. Ebara, K. Kumamoto, T. Matsuura, J. E. Mazurkiewicz, and F. L. Rice, "Similarities and differences in the innervation of mystacial vibrissal follicle–sinus complexes in the rat and cat: a confocal microscopic study," *Journal of Comparative Neurology*, vol. 449, no. 2, pp. 103–119, 2002.

[27] J.-N. Kim, K.-S. Koh, E. Lee, S.-C. Park, and W.-C. Song, "The morphology of the rat vibrissal follicle-sinus complex revealed by three-dimensional computer-aided reconstruction," *Cells Tissues Organs*, vol. 193, no. 3, pp. 207–214, 2011.

[28] L. Marotte, F. Rice, and P. Waite, "The morphology and innervation of facial vibrissae in the tammar wallaby, macropus eugenii." *Journal of anatomy*, vol. 180, no. Pt 3, p. 401, 1992.

[29] L. M. Jones, S. Lee *et al.*, "Precise temporal responses in whisker trigeminal neurons." *J. Neurophysiol*, vol. 92, no. 1, 2004.

[30] N. F. Lepora, M. J. Pearson, B. Mitchinson, M. Evans, C. Fox, A. Pipe, K. Gurney, and T. J. Prescott, "Naive bayes novelty detection for a moving robot with whiskers," in *2010 IEEE International Conference on Robotics and Biomimetics*. IEEE, 2010, pp. 131–136.

[31] M. J. Pearson and M. Salman, "Active whisker placement and exploration for rapid object recognition," 2020.

[32] M. Lungarella, V. V. Hafner, R. Pfeifer, and H. Yokoi, "An artificial whisker sensor for robotics," in *IEEE/RSJ International Conference on Intelligent Robots and Systems*, vol. 3. IEEE, 2002, pp. 2931–2936.

[33] N. H. Nguyen, T. D. Ngo, D. Q. Nguyen *et al.*, "Contact distance estimation by a soft active whisker sensor based on morphological computation," in *2020 8th IEEE RAS/EMBS International Conference for Biomedical Robotics and Biomechatronics (BioRob)*. IEEE, pp. 322–327.

[34] D. Kim and R. Moller, "Biomimetic whiskers for shape recognition," *Robotics and Autonomous Systems*, vol. 55, no. 3, pp. 229–243, 2007.

[35] N. F. Lepora, "Biomimetic active touch with fingertips and whiskers," *IEEE transactions on haptics*, vol. 9, no. 2, pp. 170–183, 2016.

[36] J. Delamare, R. Sanders, and G. Krijnen, "3d printed biomimetic whisker-based sensor with co-planar capacitive sensing," in *2016 IEEE SENSORS*. IEEE, 2016, pp. 1–3.

[37] W. Deer and P. E. Pounds, "Lightweight whiskers for contact, pre-contact, and fluid velocity sensing," *IEEE Robotics and Automation Letters*, vol. 4, no. 2, pp. 1978–1984, 2019.

[38] H. Wegiriya, N. Sornkarn, H. Bedford, and T. Nanayakkara, "A biologically inspired multimodal whisker follicle," in *Systems, Man, and Cybernetics (SMC), 2016 IEEE International Conference on*. IEEE, 2016, pp. 003 847–003 852.

[39] K. Hutson and R. Masterton, "The sensory contribution of a single vibrissa's cortical barrel," *Journal of neurophysiology*, vol. 56, no. 4, pp. 1196–1223, 1986.

[40] R. A. Brooks, "A robot that walks; emergent behaviors from a carefully evolved network," *Neural computation*, vol. 1, no. 2, pp. 253–262, 1989.

[41] T. Tsujimura and T. Yabuta, "Object detection by tactile sensing method employing force/torque information," *IEEE Transactions on robotics and Automation*, vol. 5, no. 4, pp. 444–450, 1989.

[42] M. Kaneko, N. Kanayama, and T. Tsuji, "Active antenna for contact sensing," *Robotics and Automation, IEEE Transactions on*, vol. 14, no. 2, pp. 278–291, 1998.

[43] R. A. Russell, "Closing the sensor-computer-robot control loop," *Robotics Age*, vol. 6, no. 4, pp. 15–20, 1984.

[44] R. A. Russell and J. A. Wijaya, "Object exploration using whisker sensors," *Australasian Conference on Robotics and Automation*, pp. 180–185, 2002.

[45] M. Fend, "Whisker-based texture discrimination on a mobile robot," *Advances in Artificial Life*, vol. 3630 of the series Lecture Notes in Computer Science, pp. 302–311, 2005.

[46] J. H. Solomon and M. J. Hartmann, "Robotic whiskers used to sense features," *Nature*, vol. 443, no. 7111, p. 525, 2006.

[47] M. Pearson, B. Mitchinson *et al.*, "Biomimetic vibrissal sensing for robots." *Phil. Trans. R. Soc. B*, vol. 366, no. 1581, 2011.

[48] J. H. Solomon and M. J. Hartmann, "Artificial whiskers suitable for array implementation: accounting for lateral slip and surface friction," *IEEE Transactions on Robotics*, vol. 24, no. 5, pp. 1157–1167, 2008.

[49] A. Kottapalli, M. Asadnia, J. Miao, and M. Triantafyllou, "Harbor seal whisker inspired flow sensors to reduce vortex-induced vibrations," in *2015 28th IEEE International Conference on Micro Electro Mechanical Systems (MEMS)*. IEEE, 2015, pp. 889–892.

[50] J. Sullivan, M. Pearson *et al.*, "Tactile discrimination using active whisker sensors," *IEEE Sensors*, vol. 12, no. 2, pp. 350–362, 2012.

[51] L. Sun, S. Rogers, G. Aragon-Camarasa, and J. P. Siebert, "Recognising the clothing categories from free-configuration using gaussian-process-based interactive perception," in *2016 IEEE International Conference on Robotics and Automation (ICRA)*. IEEE, 2016, pp. 2464–2470.

[52] N. Jamali and C. Sammut, "Material classification by tactile sensing using surface textures," in *2010 IEEE International Conference on Robotics and Automation*. IEEE, 2010, pp. 2336–2341.

[53] L. Sharan, C. Liu, R. Rosenholtz, and E. H. Adelson, "Recognizing materials using perceptually inspired features," *International journal of computer vision*, vol. 103, no. 3, pp. 348–371, 2013.

[54] J. H. Solomon and M. J. Hartmann, "Robotic whiskers used to sense features," *Nature*, vol. 443, no. 7111, pp. 525–525, 2006.

[55] P. Allen, "Surface descriptions from vision and touch," in *Proceedings. 1984 IEEE International Conference on Robotics and Automation*, vol. 1. IEEE, 1984, pp. 394–397.

[56] R. A. Russell, "Using tactile whiskers to measure surface contours," in *Proceedings 1992 IEEE International Conference on Robotics and Automation*. IEEE, 1992, pp. 1295–1299.

[57] J. H. Solomon and M. J. Hartmann, "Extracting object contours with the sweep of a robotic whisker using torque information," *The International Journal of Robotics Research*, vol. 29, no. 9, pp. 1233–1245, 2010.

[58] T. Hoinville, N. Harischandra, A. F. Krause, and V. Dürr, "Insect-inspired tactile contour sampling using vibration-based robotic antennae," in *Conference on Biomimetic and Biohybrid Systems*. Springer, 2014, pp. 118–129.

[59] M. J. Pearson, B. Mitchinson, J. C. Sullivan, A. G. Pipe, and T. J. Prescott, "Biomimetic vibrissal sensing for robots," *Philosophical Transactions of the Royal Society B: Biological Sciences*, vol. 366, no. 1581, pp. 3085–3096, 2011.

[60] M. J. Pearson, A. G. Pipe, C. Melhuish, B. Mitchinson, and T. J. Prescott, "Whiskerbot: A robotic active touch system modeled on the rat whisker sensory system," *Adaptive Behavior*, vol. 15, no. 3, pp. 223–240, 2007.

[61] T. N. Clements and C. D. Rahn, "Three-dimensional contact imaging with an actuated whisker," *IEEE Transactions on robotics*, vol. 22, no. 4, pp. 844–848, 2006.

[62] L. Zhu, L. Zeng, X. Chen, X. Luo, and X. Li, "A bioinspired touching sensor for amphibious mobile robots," *Advanced Robotics*, vol. 29, no. 22, pp. 1437–1452, 2015.

[63] M. Fend, S. Bovet, H. Yokoi, and R. Pfeifer, "An active artificial whisker array for texture discrimination," in *Proceedings 2003 IEEE/RSJ International Conference on Intelligent Robots and Systems (IROS 2003)(Cat. No. 03CH37453)*, vol. 2. IEEE, 2003, pp. 1044–1049.

[64] M. Fend, "Whisker-based texture discrimination on a mobile robot," in *European Conference on Artificial Life*. Springer, 2005, pp. 302–311.

[65] J. Hipp, E. Arabzadeh, E. Zorzin, J. Conradt, C. Kayser, M. E. Diamond, and P. Konig, "Texture signals in whisker vibrations," *Journal of neurophysiology*, vol. 95, no. 3, pp. 1792–1799, 2006.

[66] M. Evans, C. W. Fox, M. J. Pearson, and T. J. Prescott, "Spectral template based classification of robotic whisker sensor signals in a floor texture discrimination task," *Proceedings TAROS*, pp. 19–24, 2009.

[67] J. C. Sullivan, B. Mitchinson, M. J. Pearson, M. Evans, N. F. Lepora, C. W. Fox, C. Melhuish, and T. J. Prescott, "Tactile discrimination using active whisker sensors," *IEEE Sensors Journal*, vol. 12, no. 2, pp. 350–362, 2011.

[68] N. F. Lepora, M. Pearson, and L. Cramphorn, "Tacwhiskers: Biomimetic optical tactile whiskered robots," in *2018 IEEE/RSJ International Conference on Intelligent Robots and Systems (IROS)*. IEEE, 2018, pp. 7628–7634.

[69] S. NGuyen, P. Pirim, and J.-A. Meyer, "Texture discrimination with artificial whiskers in the robot-rat psikharpax," in *International Joint Conference on Biomedical Engineering Systems and Technologies*. Springer, 2010, pp. 252–265.

[70] J. Steigenberger, C. Behn, and C. Will, *Mathematical model of vibrissae for surface texture detection*. Techn. Univ., Inst. für Mathematik, 2015.

[71] Y. Boubenec, L. N. Claverie, D. E. Shulz, and G. Debrégeas, "An amplitude modulation/demodulation scheme for whisker-based texture perception," *Journal of neuroscience*, vol. 34, no. 33, pp. 10 832–10 843, 2014.

[72] M. Fend, S. Bovet, and V. Hafner, "The artificial mouse-a robot with whiskers and vision," in *Proceedings of the 35th International Symposium on Robotics (ISR 2004)*. Citeseer, 2004.

[73] T. Schlegl, T. Kröger, A. Gaschler, O. Khatib, and H. Zangl, "Virtual whiskershighly responsive robot collision avoidance," in *2013 IEEE/RSJ International Conference on Intelligent Robots and Systems*. IEEE, 2013, pp. 5373–5379.

[74] J. P. Grotzinger, J. Crisp, A. R. Vasavada, R. C. Anderson, C. J. Baker, R. Barry, D. F. Blake, P. Conrad, K. S. Edgett, B. Ferdowski *et al.*, "Mars science laboratory mission and science investigation," *Space science reviews*, vol. 170, no. 1-4, pp. 5–56, 2012.

[75] J. Maki, J. Bell, K. E. Herkenhoff, S. Squyres, A. Kiely, M. Klimesh, M. Schwochert, T. Litwin, R. Willson, A. Johnson *et al.*, "Mars exploration rover engineering cameras," *Journal of Geophysical Research: Planets*, vol. 108, no. E12, 2003.

[76] C. Zhao, Q. Jiang, and Y. Li, "A novel biomimetic whisker technology based on fiber bragg grating and its application," *Measurement Science and Technology*, vol. 28, no. 9, p. 095104, 2017.

[77] N. J. Cowan, E. J. Ma, M. Cutkosky, and R. J. Full, "A biologically inspired passive antenna for steering control of a running robot," in *Robotics Research. The Eleventh International Symposium*. Springer, 2005, pp. 541–550.

[78] D. B. Zurek and C. Gilbert, "Static antennae act as locomotory guides that compensate for visual motion blur in a diurnal, keen-eyed predator," *Proceedings of the Royal Society B: Biological Sciences*, vol. 281, no. 1779, p. 20133072, 2014.

[79] P. Giguere and G. Dudek, "A simple tactile probe for surface identification by mobile robots," *IEEE Transactions on Robotics*, vol. 27, no. 3, pp. 534–544, 2011.

[80] M. Salman and M. J. Pearson, "Advancing whisker based navigation through the implementation of bio-inspired whisking strategies," in *2016 IEEE International Conference on Robotics and Biomimetics (ROBIO)*. IEEE, 2016, pp. 767–773.

[81] V. Feliu-Batlle, D. Feliu-Talegon, and C. F. Castillo-Berrio, "Improved object detection using a robotic sensing antenna with vibration damping control," *Sensors*, vol. 17, no. 4, p. 852, 2017.

[82] P. Hebert, N. Hudson, J. Ma, and J. Burdick, "Fusion of stereo vision, force-torque, and joint sensors for estimation of in-hand object location," in *2011 IEEE International Conference on Robotics and Automation*. IEEE, 2011, pp. 5935–5941.

[83] T. Rooney, M. Pearson, J. Welsby, I. Horsfield, R. Sewell, and S. Dogramadzi, "Artificial active whiskers for guiding underwater autonomous walking robots," 2011.

[84] M. Björkman, Y. Bekiroglu, V. Högman, and D. Kragic, "Enhancing visual perception of shape through tactile glances," in *2013 IEEE/RSJ International Conference on Intelligent Robots and Systems*. IEEE, 2013, pp. 3180–3186.

[85] P. Güler, Y. Bekiroglu, X. Gratal, K. Pauwels, and D. Kragic, "What's in the container? classifying object contents from vision and touch," in *2014 IEEE/RSJ International Conference on Intelligent Robots and Systems*. IEEE, 2014, pp. 3961–3968.

[86] J. Ilonen, J. Bohg, and V. Kyrki, "Fusing visual and tactile sensing for 3-d object reconstruction while grasping," in *2013 IEEE International Conference on Robotics and Automation*. IEEE, 2013, pp. 3547–3554.

[87] C. MacLeod, J. Cao, S. Pierce, J. Sullivan, A. Pipe, G. Dobie, and R. Summan, "Remotely deployable aerial inspection using tactile sensors," in *AIP Conference Proceedings*, vol. 1581, no. 1. American Institute of Physics, 2014, pp. 1873–1880.

[88] O. Bebek and M. C. Cavusoglu, "Whisker sensor design for three dimensional position measurement in robotic assisted beating heart surgery," in *Proceedings 2007 IEEE International Conference on Robotics and Automation*. IEEE, 2007, pp. 225–231.

[89] H. Takahashi-Iwanaga, "Three-dimensional microanatomy of longitudinal lanceolate endings in rat vibrissae," *Journal of Comparative Neurology*, vol. 426, no. 2, pp. 259–269, 2000.

[90] F. L. Rice, A. Mance, and B. L. Munger, "A comparative light microscopic analysis of the sensory innervation of the mystacial pad. i. innervation of vibrissal follicle-sinus complexes," *Journal of Comparative Neurology*, vol. 252, no. 2, pp. 154–174, 1986.

[91] M. Szwed, K. Bagdasarian, and E. Ahissar, "Encoding of vibrissal active touch," *Neuron*, vol. 40, no. 3, pp. 621–630, 2003.

[92] L. Pammer, D. H. O'Connor, S. A. Hires, N. G. Clack, D. Huber, E. W. Myers, and K. Svoboda, "The mechanical variables underlying object localization along the axis of the whisker," *Journal of Neuroscience*, vol. 33, no. 16, pp. 6726–6741, 2013.

[93] N. Sornkarn, M. Howard, and T. Nanayakkara, "Internal impedance control helps information gain in embodied perception," in *Robotics and Automation (ICRA), 2014 IEEE International Conference on*. IEEE, 2014, pp. 6685–6690.

[94] L. A. Huet, J. W. Rudnicki, and M. J. Hartmann, "Tactile sensing with whiskers of various shapes: Determining the three-dimensional location of object contact based on mechanical signals at the whisker base," *Soft Robotics*, vol. 4, no. 2, pp. 88–102, 2017.

[95] M. Baatz and M. Hyrenbach, "Method of calculating the magnetic flux density and forces in contactfree magnetic bearings," Jul. 1991. [Online]. Available: https://onlinelibrary.wiley.com/doi/abs/10.1002/etep.4450010404

[96] B. Balachandran and E. B. Magrab, *Vibrations*, 2nd ed. Australia: Cengage Learning, 2009, oCLC: ocn181603380.

[97] E. B. Magrab, *An engineer's guide to MATLAB: with applications from mechanical, aerospace, electrical, civil, and biological systems engineering*, 3rd ed. Upper Saddle River, N.J: Prentice Hall, 2011, oCLC: ocn465867437.

[98] D. S. Chathuranga, Z. Wang, Y. Noh, T. Nanayakkara, and S. Hirai, "Robust real time material classification algorithm using soft three axis tactile sensor: Evaluation of the algorithm," in *Intelligent Robots and Systems (IROS), 2015 IEEE/RSJ International Conference on*. IEEE, 2015, pp. 2093–2098.

[99] D. S. Chathuranga, Z. Wang, Y. Noh, , T. Nanayakkara, and S. Hirai, "Disposable soft 3 axis force sensor for biomedical applications," in *Engineering in Medicine and Biology Society (EMBC), 2015 37th Annual International Conference of the IEEE*. IEEE, 2015, pp. 5521–5524.

[100] A. G. Lamperski, O. Y. Loh, B. L. Kutscher, and N. J. Cowan, "Dynamical wall following for a wheeled robot using a passive tactile sensor," in *Robotics and Automation, 2005. ICRA 2005. Proceedings of the 2005 IEEE International Conference on*. IEEE, 2005, pp. 3838–3843.

[101] A. Wallach, K. Bagdasarian, and E. Ahissar, "On-going computation of whisking phase by mechanoreceptors," *Nature neuroscience*, vol. 19, no. 3, p. 487, 2016.

[102] D. Campagner, M. H. Evans, M. S. Loft, and R. S. Petersen, "What the whiskers tell the brain," *Neuroscience*, vol. 368, pp. 95–108, 2018.

[103] E. Arabzadeh, R. S. Petersen, and M. E. Diamond, "Encoding of whisker vibration by rat barrel cortex neurons: implications for texture discrimination," *Journal of Neuroscience*, vol. 23, no. 27, pp. 9146–9154, 2003.

[104] F. Ju and S.-F. Ling, "Bioinspired active whisker sensor for robotic vibrissal tactile sensing," *Smart Materials and Structures*, vol. 23, no. 12, p. 125003, 2014.

[105] N. Sornkarn and T. Nanayakkara, "The efficacy of interaction behavior and internal stiffness control for embodied information gain in haptic perception," in *Robotics and Automation (ICRA), 2016 IEEE International Conference on.* IEEE, 2016, pp. 2657–2662.